Article:
Claussmann, B, Bailleul, J, Chanier, F et al. (3 more authors) (2023) Early stages of trench-slope basin development: Insights from mass-transport deposits and their interactions with turbidite systems (southern Hikurangi margin, New Zealand). Marine and Petroleum Geology, 152. 106191. ISSN 0264-8172

https://doi.org/10.1016/j.marpetgeo.2023.106191

Early stages of trench-slope basin development: insights from mass-transport deposits and their interactions with turbidite systems (southern Hikurangi margin, New Zealand)

Claussmann B.[1,2,*], Bailleul J.[2], Chanier F.[3], Mahieux G.[4], McArthur A. D.[5], Vendeville B. C.[3]

1. SLB, Digital Subsurface Solutions, Abingdon, OX14 4RU, United Kingdom
2. U2R 7511, Basins-Reservoirs-Resources (B2R), Geosciences department, UniLaSalle - University of Picardie Jules Verne, 60026, Beauvais, France
3. University of Lille, CNRS, ULCO, UMR 8187, Laboratory of Oceanology and Geosciences (LOG), Lille, France
4. U2R 7511, Basins-Reservoirs-Resources (B2R), University of Picardie Jules Verne - UniLaSalle, 80039 Amiens, France
5. School of Earth and Environment, University of Leeds, Leeds, LS2 9JT, United Kingdom

Accepted Manuscript version (unedited PDF accepted for publication).

Published Journal Article version available online, 2 March 2023:

https://doi.org/10.1016/j.marpetgeo.2023.106191

Personalized URL providing free access to the article until May 31, 2023:

https://authors.elsevier.com/a/1guypyDcGWUEB

Published by Elsevier in Marine and Petroleum Geology Journal.

*Correspondence: bclaussmann@slb.com

ABSTRACT

Geological complexity, progressive tectonic overprint and prevailing submarine location of subduction margins generally hinder investigating the early stages of development of their oldest trench-slope basins, witnesses of subduction initiation and early history. Along the eastern North Island of New Zealand, the inner portion of the Hikurangi subduction wedge is emerged, thereby offering a unique opportunity to examine, at outcrop-scale, the tectonostratigraphic evolution of a trench-slope basin (Castlepoint trench-slope basin) that was linked to the onset of subduction. We present new occurrences of lowermost Miocene gravity-driven systems, suggesting a more intricate depositional framework to the ones previously inferred during this key period. Results show that the early stages of development of a trench-slope basin coeval with the birth of a subduction margin may deviate from traditional models either comprising (1) sustainable sediment sources connected to the basin very early in the history of the margin and (2) a sedimentation-deformation feedback mechanism promoting the long-term development of an aggradational turbidite system downslope. Analysis of the mass-transport deposits (MTDs) also revealed that the outboard migration of deformation was discontinuous and uneven along the margin during the earliest Miocene. Two major tectonic events, separated by a period of reduced tectonic activity, were recorded at the inboard border of the Castlepoint trench-slope basin, each resulting in seaward motion, oversteepening and frontal denudation of a thrust sheet. Each thrust sheet provided contrasting failed material and morphometric characteristics to the associated deposits, thereby allowing us to discriminate the nature of the nappe and related controls responsible for shedding each MTD as well as refine the timing of nappe emplacement along this part of the margin. Overall, this study draws new insights on the early structural evolution and stratigraphic infill during the birth of subduction zones, insights which may, in turn, help improve understandings of active margin settings.

Keywords: active margin, gravity-driven deposits, mass-wasting system, confined basins, trench-slope basins, thrust forelimb, channel levee system, olistostrome

1. INTRODUCTION

Trench-slope basins are confined intra-slope basins that develop along all subduction margins (*e.g.,* Karig and Sharman 1975; Moore and Karig 1976; Smith et al. 1979; Karig et al. 1980; Moore et al. 1980; White and Louden 1982; Stevens and Moore 1985; Underwood and Norville 1986; Okada 1989; McCrory 1995; Underwood and Moore 1995) and more particularly on their subduction wedge (*sensu* Bailleul et al. 2013). Trench-slope basins typically form narrow, elongate and trench-parallel structural depressions separated by tectonically active bathymetric highs that are by-products of seaward-verging thrust faulting and asymmetrical folding (Moore and Karig 1976; Karig et al. 1980; Moore et al. 1980; Stevens and Moore 1985; Okada 1989; Underwood and Moore 1995).

Located between the trench and the trench-slope break (*i.e.,* on the lower trench-slope of a margin), these intra-slope basins are progressively uplifted and migrate upslope through time, moving away from the deformation front, owing to the seaward expansion and growth of the subduction wedge (Underwood and Moore 1995). As a result, at their early stages of development, trench-slope basins are generally located towards the base of the lower trench-slope. There, they are more likely to be sedimentologically 'immature' (*sensu* Underwood and Bachman 1982), being disconnected from the main sediment pathways that cross the margin, and thus typically comprise hemipelagic deposits or remobilized material, slumped off from the adjacent bathymetric highs (Moore and Karig 1976). As they migrate upslope however, they generally become sedimentologically 'mature' (*sensu* Underwood and Bachman 1982) being connected to the terrigenous sediment input and thus, chiefly trap coarser-grained, gravity-driven material.

In the past twenty years, numerous studies highlighted that owing to the strong interplay that exists between deformation and sedimentation in such tectonically active settings, more diversified and complicated frameworks could be drawn for the tectonostratigraphic evolution of trench-slope basins (*e.g.,* Underwood et al. 2003; Bailleul et al. 2007; Vinnels et al. 2010; Bailleul et al. 2013; Noda 2018; McArthur et al. 2019). Indeed, their development, distribution, geometry and stratigraphic infill were recurrently observed to be strongly influenced by the contemporaneous structural growth of the subduction wedge driven by subduction processes and their variations through time (*e.g.,* Bailleul et al. 2013; Ghisetti et al. 2016; Noda 2018).

Despite numerous studies of subduction margin settings, their complexity, progressive tectonic overprint and prevailing submarine location hinder investigating the early stages of development of the margins' oldest trench-slope basins. Therefore, bringing new elements to address this knowledge gap may

Accepted Manuscript version. Published Journal Article version available online, published by Elsevier in Marine and Petroleum Geology Journal: https://doi.org/10.1016/j.marpetgeo.2023.106191

constitute a milestone for the understanding of active margins, and more particularly for those trench-slope basins that are contemporaneous with the birth of subduction zones.

Along the eastern North Island of New Zealand, the western, exhumed, inner portion of the Hikurangi subduction wedge (*i.e.,* the coastal ranges) is partly emerged (Figure 1), and therefore offers an opportunity to investigate, at outcrop-scale, the tectonostratigraphic evolution of the first trench-slope basins (*e.g.,* the Castlepoint trench-slope basin) that were linked to the onset of subduction in the earliest Miocene (eventually latest Oligocene) (*e.g.,* van der Lingen and Pettinga 1980; van der Lingen 1982; Chanier and Ferrière 1991; Neef 1992a; Lewis and Pettinga 1993; Bailleul et al. 2007; Bailleul et al. 2013; McArthur et al. 2019). Previous outcrop-based studies revealed that the abrupt changes of structural and sedimentation styles recorded during this short period of intense deformation (~3-5 Myr) resulted from (1) the seaward emplacement of a succession of thrust sheets underwater and (2) sudden high sediment input of detrital material, primarily distributed through gravity-driven systems into the newly formed trench-slope basins (Chanier and Ferrière 1991; Rait et al. 1991).

The associated lowermost Miocene deposits, known as the Whakataki Formation, were extensively described in the coastal ranges, and more particularly within the coastal Castlepoint trench-slope basin (Van den Heuvel 1960; Johnston 1980; Chanier and Ferrière 1991; Neef 1992; Neef 1995; Neef 1995; Edbrooke and Browne 1996; Delteil et al. 1996; Field et al. 1997; Neef 1997; Lee and Begg 2002; Field 2005; Delteil et al. 2006; Bailleul et al. 2007; Bailleul et al. 2013; Down 2016; Malie et al. 2017; Sloss et al. 2021). They mostly comprise deep-marine, fine-grained turbidites occasionally interrupted by mass-transport deposits (MTDs), at the base or near the base of the series, ascribed to result from the frontal erosion of the advancing thrust sheets before turbiditic sedimentation took over (*e.g.,* Johnston 1980; Chanier and Ferrière 1991; Lee and Begg 2002; Field 2005).

In this study, we report newly described occurrences of the lowermost Miocene sediments in the Castlepoint trench-slope basin, which suggest a more complicated depositional framework. The associated deposits are superbly exposed at low tide to the south of the Castlepoint area, along more than 14 kilometers of wavecut platform. These successions record both the long-term development of a several hundreds of meters thick aggradational channel-levee complex system and the emplacement of three distinct styles of large-scale MTDs.

This study aims to combine these new insights with previous studies along an 80 kilometer-long coastal transect across the partially emerged Castlepoint trench-slope basin (Figure 2) to (1) better comprehend the early stages of tectonostratigraphic development of a trench-slope basin contemporaneous with the

Accepted Manuscript version. Published Journal Article version available online, published by Elsevier in Marine and Petroleum Geology Journal: https://doi.org/10.1016/j.marpetgeo.2023.106191

birth of a subduction zone and (2) investigate the role of MTDs as spatial-temporal markers of geologic events in such a context.

Here, the lateral and vertical variabilities of the MTDs as well as their interactions with the turbidite systems not only suggest that different controlling parameters influenced their styles but also that the subsequent deposits captured the lateral and longitudinal evolution of the trench-slope basin-bounding structures (*e.g.,* thrusts and growing anticlines).

Specific objectives are to:

- Describe the internal characteristics and architectures of different styles of gravity-driven systems, which can occur in the early-stage fill of a trench-slope basin.
- Document the diversity of MTDs, which can develop at the front of thrust faults to gain new insights into the different mass-wasting processes and causal mechanisms, which were involved in their development, emplacement and preservation.
- Use detailed analysis of the MTDs, their failed material and their interactions with the turbidite systems as a tool to discriminate the nature of the thrust sheets involved in each of the MTDs and specify the timing of nappe emplacement along the Hikurangi Margin.
- Construct a generic depositional model capturing the distribution, styles as well as the processes and controls that influence MTDs at the front of thrust faults.

Accepted Manuscript version. Published Journal Article version available online, published by Elsevier in Marine and Petroleum Geology Journal: https://doi.org/10.1016/j.marpetgeo.2023.106191

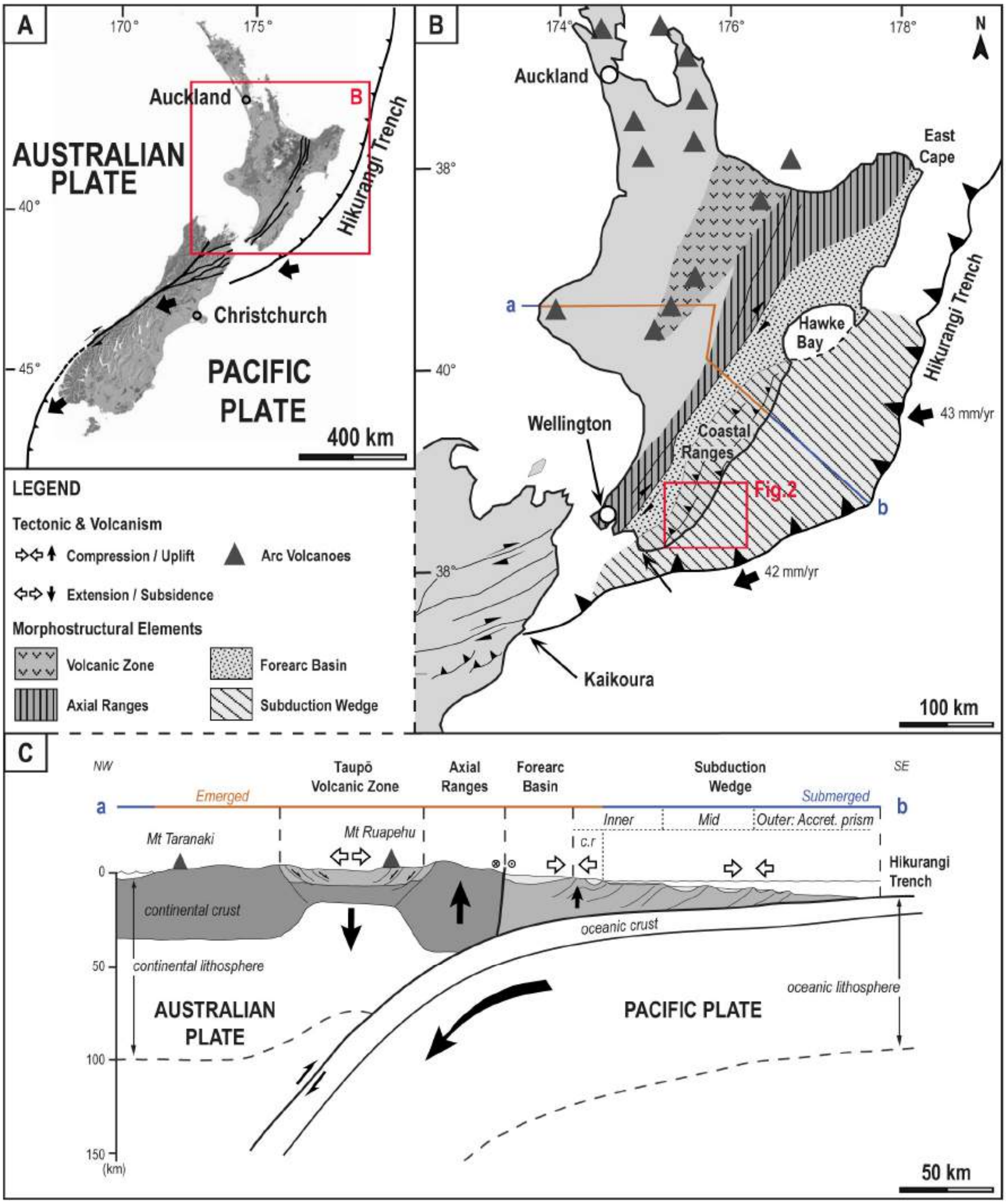

Figure 1: (A): Plate tectonic setting of New Zealand. (B): Major subduction-related morphostructural features of the Hikurangi active margin, North Island of New Zealand. Black arrows show present-day relative plate motion between Pacific and Australian plates from Beavan et al. (2002). See (C) for the a – b general cross-section of the Hikurangi subduction complex (c.r – coastal ranges). Modified after Chanier et al. (1999), Bailleul et al. (2007) and Bailleul et al. (2013).

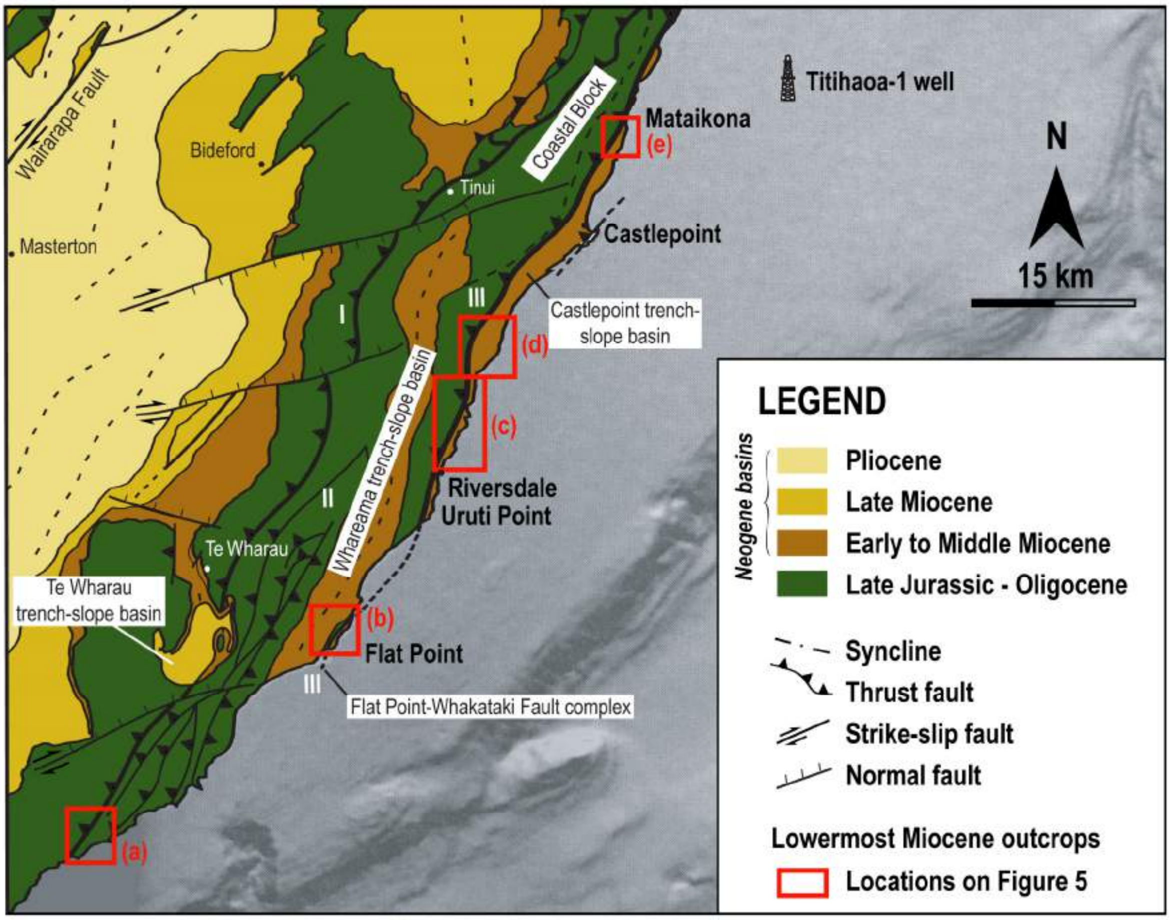

Figure 2: Bathymetric map (Lewis et al. 1999) and onshore structural map (modified from Chanier et al. (1999), Lee and Begg (2002) and Bailleul et al. (2013)) of the southern Hikurangi subduction wedge. The offshore area includes the location of the well Titihaoa-1 (Biros et al. 1995; Griffin et al. 2022). Locations of the fault complexes = (I): Adams-Tinui Fault complex, (II): Pukeroro Fault, (III): Flat Point-Whakataki Fault complex to the south, known to evolve into the Whakataki-Turnagain Fault complex to the north. Locations of the lowermost Miocene [NZ stage: late Waitakian-Otaian] coastal sections = (a): Pahaoa section, (b): Flat Point section, (c): Orui sections, (d): Waimimi sections and (e): Suicide Point-Mataikona section.

2. GEOLOGICAL SETTING

2.1. Tectonostratigraphic record of the Hikurangi subduction onset

About 25-21 Ma ago, the eastern North Island of New Zealand was the scene of a major geodynamic change, transitioning from a tectonically passive to active setting (Chanier 1991; Rait et al. 1991; King 2000; Hayward et al. 2001; Nicol et al. 2007; Bland et al. 2022; Hines et al. 2022). The westward subduction of the Pacific Plate beneath the Australian Plate (1) marked the end of a sustained period of tectonic quiescence that lasted from the Late Cretaceous to the Oligocene and (2) controlled the complex and polyphase tectonostratigraphic development of the Hikurangi subduction wedge from its onset in the earliest Miocene (or eventually latest Oligocene) (Figure 1; Figure 3) (Ballance 1976; Spörli 1980; Pettinga 1982; Chanier and Ferrière 1991; Rait et al. 1991; Field et al. 1997; Nicol et al. 2007).

Bounded by the Hikurangi Trench to the east and the forearc basin *sensu stricto* to the west, the Hikurangi subduction wedge is composed of a series of elongated sedimentary basins (*i.e.,* trench-slope basins (*sensu* Underwood and Moore 1995)) separated by trench-parallel structural ridges that exert or have exerted a crucial control on their Miocene-to-Recent stratigraphic infills (Figure 1) (Chanier and Ferrière 1991; Lewis and Pettinga 1993; Bailleul et al. 2013; Bland et al. 2015; Ghisetti et al. 2016; McArthur et al. 2019; Claussmann et al. 2021; Claussmann et al. 2022; Griffin et al. 2022).

The development of the Hikurangi subduction wedge started at the onset of subduction with a major episode of SE-directed compressional deformation that resulted in the seaward emplacement of a succession of thrust sheets involving the Lower Cretaceous to Oligocene series of the pre-subduction margin (Figure 3; Figure 4) (Pettinga 1982; Chanier and Ferrière 1989; Chanier and Ferrière 1991; Rait et al. 1991). At the onset of subduction, the plate convergence was rapid (~80 millimeters/year) (Chanier 1991), with an estimated total shortening across the margin in excess of 25 kilometers (Nicol et al. 2007; Hines et al. 2022). The remobilized pre-subduction margin series eventually formed a succession of superposed nappes (each between 0.2-1.5 kilometers thick) with eastward overthrusting of the Lower Cretaceous over the Upper Cretaceous to Oligocene proximal units, themselves overthrusting more distal units (Figure 4A) (Chanier and Ferrière 1989; Chanier and Ferrière 1991; Rait et al. 1991).

Abrupt changes of sedimentation styles and rates were also recorded during this particular period of nappe emplacement, with a syn-subduction detrital sedimentation dominated by deep-marine gravity-

Accepted Manuscript version. Published Journal Article version available online, published by Elsevier in Marine and Petroleum Geology Journal: https://doi.org/10.1016/j.marpetgeo.2023.106191

driven systems that radically contrasts with the previous Eocene-Oligocene pelagic sedimentation (Chanier and Ferrière 1991; Field et al. 1997; Morgans 2016).

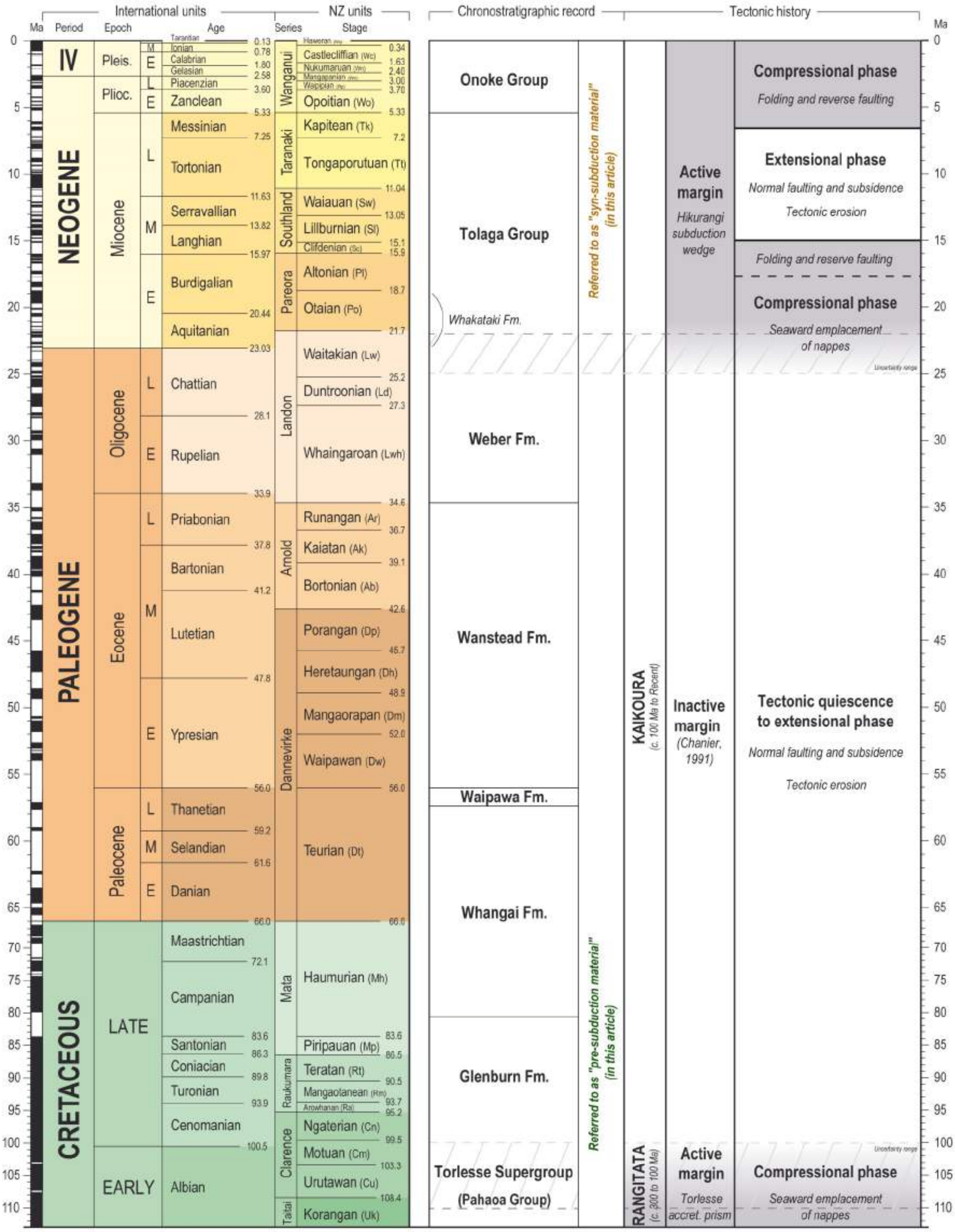

Figure 3: Chronostratigraphic chart for the southern emerged portion of the Hikurangi subduction wedge. Stratigraphy of the pre- and syn-Hikurangi subduction series adapted from (Chanier 1991; Chanier and Ferrière 1991; Field et al. 1997; Lee and Begg 2002; Bland et al. 2015; Bland et al. 2022). Regional tectonism adapted from Chanier et al. (1999), Bailleul et al.

Accepted Manuscript version. Published Journal Article version available online, published by Elsevier in Marine and Petroleum Geology Journal: https://doi.org/10.1016/j.marpetgeo.2023.106191

(2013) and Malie et al. (2017). New Zealand stages after Raine et al. (2015) showing the equivalence with the international stages.

The resulting deposits date from the earliest Miocene, late Waitakian to Otaian (Aquitanian to Early Burdigalian, 23.03 – 18.7 Ma) and belong to the Whakataki Formation (Johnston 1980). They characteristically consist of up to 1,500 meters of deep-marine, mainly fine-grained, turbidites occasionally interrupted by a few meters up to several hundred of meters thick MTDs at or near the base of the formation (*e.g.,* Johnston 1980; Chanier and Ferrière 1991; Lee and Begg 2002; Field 2005). The Whakataki Formation locally overlies the pre-subduction margin series conformably, thereby suggesting that its deposition was closely linked to the event of thrust sheets' emplacement, for which propagation lasted about three to five million years (from late Waitakian to late Otaian) (Chanier and Ferrière 1991; Rait et al. 1991).

2.2. Stratigraphy of the pre-subduction margin series

The pre-subduction margin series comprise (1) the Upper Cretaceous to Oligocene passive margin strata, which shows an eastward evolution from detrital (proximal, to the west) to pelagic (distal, to the east) sedimentation (Figure 4) (Johnston 1980; Moore 1986; Chanier 1991; Chanier and Ferrière 1991; Crampton 1997; Field et al. 1997; Lee and Begg 2002; Morgans 2016; Hines 2018) and (2) the Jurassic to Lower Cretaceous Torlesse Supergroup (Figure 3; Figure 4) (Suggate 1961; George 1990; George 1992), remnant of an older accretionary prism that forms the underlying basement (Figure 4B) (Spörli 1980; Bradshaw 1989; Mortimer 2004; Mortimer et al. 2014; Bland et al. 2015).

The Torlesse Supergroup is composed of metasedimentary rocks that mainly include heavily deformed and indurated sandstones and mudstones (greywackes and argilites) as well as sporadic red cherts, radiolarites and basalts (Spörli 1980; Bradshaw 1989; Barnes and Korsch 1990; Barnes and Korsch 1991; Mortimer 1994; Field et al. 1997). Considered a former thick sedimentary oceanic plateau, the Torlesse was strongly deformed during its subduction and accretion along the New Zealand crust (*i.e.,* former eastern Gondwana margin) until late Early Cretaceous times (*e.g.,* Spörli 1978; Bradshaw 1989; George 1992; Mortimer 2004).

Following that major orogenic period, Upper Cretaceous to Oligocene strata were deposited on top of the Torlesse basement. They can be subdivided into five main stratigraphic units: (1) the Upper Cretaceous Glenburn Formation, which can locally reach up to 1,000 meters in thickness and mostly consists of coarse detrital sedimentary rocks characterized by alternating conglomerates, sandstones and siltstones; (2) the Upper Cretaceous to Paleocene Whangai Formation, which represents about 100

Accepted Manuscript version. Published Journal Article version available online, published by Elsevier in Marine and Petroleum Geology Journal: https://doi.org/10.1016/j.marpetgeo.2023.106191

to 500 meters of massive siltstones and silty mudstones, occasionally disturbed by pebbly conglomerates, calcareous concretions, azoic glauconitic sandstone beds, sedimentary dykes, limestone lenses, and evolving from being mostly siliceous during the Upper Cretaceous to being mostly carbonated during the Paleocene; (3) the Upper Paleocene Waipawa Formation, which corresponds to a few meters up to 50 meters of organic-rich silty mudstones; (4) the Eocene Wanstead Formation, which characteristically comprises 100 to 200 meters of now weakly indurated light green, red or black calcareous and smectitic mudstones, occasionally interbedded with glauconite-rich sandstones; and finally (5) the Oligocene Weber Formation, about 200 to 340 meters thick, and generally consisting of whitish pelagic marls and limestones (Figure 3; Figure 4B) (Van den Heuvel 1960; Moore 1980; Moore 1986; Chanier and Ferrière 1991; Crampton 1997; Field et al. 1997; Lee and Begg 2002; Hines et al. 2013; Hollis et al. 2014; Bland et al. 2015; Morgans 2016; Crampton et al. 2019).

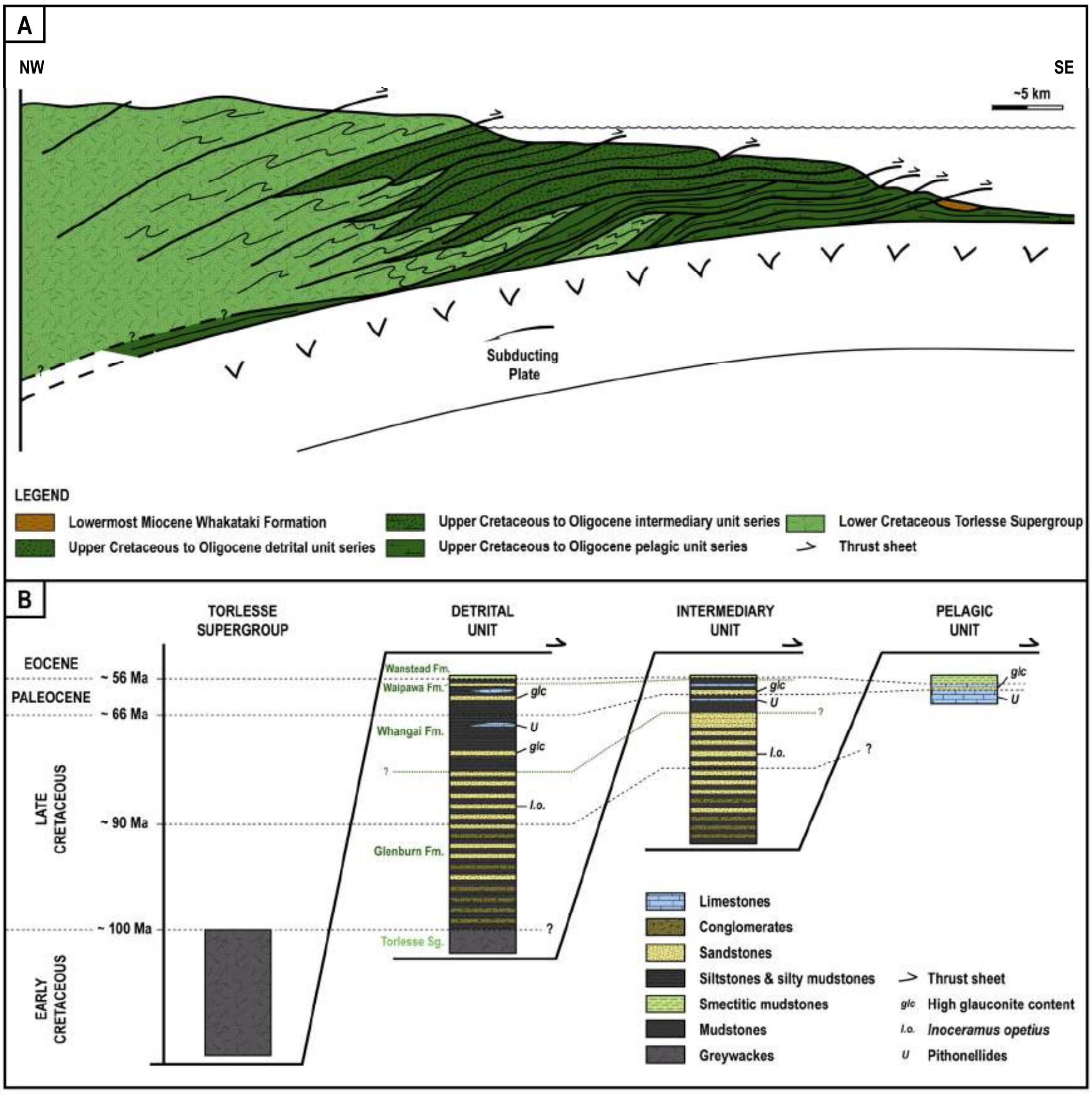

Accepted Manuscript version. Published Journal Article version available online, published by Elsevier in Marine and Petroleum Geology Journal: https://doi.org/10.1016/j.marpetgeo.2023.106191

Figure 4: [previous page] (A): Schematic cross-section from Chanier (1991) representing the development of the Hikurangi subduction wedge at the onset of subduction in the earliest Miocene. This onset was marked by the seaward emplacement of a series of thrust sheets that involved and stacked the pre-subduction margin series. (B): The pre-subduction margin series can be divided into (1) the Lower Cretaceous Torlesse greywackes and (2) the Upper Cretaceous to Oligocene strata, evolving from detrital to intermediary to pelagic sediments eastward (Johnston 1980; Spörli 1980; Moore 1986; Bradshaw 1989; Chanier 1991; Chanier and Ferrière 1991; Mortimer 1994; Crampton 1997; Field et al. 1997; Lee and Begg 2002; Lee and Begg 2002; Mortimer et al. 2014).

The easternmost pelagic series of the passive margin typically comprises (1) up to 10 meters of white to pink-grey micritic and Pithonellid-bearing limestones in the Late Cretaceous (Chanier et al. 1990) as well as (2) 20 to 90 meters of whitish micritic limestones (Kaiwhata limestones) in the Paleocene (Figure 4B, pelagic unit) (Van den Heuvel 1960; Chanier and Ferrière 1991; Lee and Begg 2002; Hines et al. 2013).

2.3. Syn-subduction lowermost Miocene MTDs

In this study, we specifically focus on the lowermost Miocene mass-wasting processes that remobilized the pre-subduction margin series. Previous field studies informed that the related MTDs (*i.e.,* olistostromes (*sensu* Flores 1955) or sedimentary mélanges (*sensu* Raymond 1984)) are mappable units of matrix-supported pebbly conglomerates that essentially rework pre-subduction material, randomly scattered within a silty mudstone- to siltstone-dominated matrix (Chanier and Ferrière 1991; Lee and Begg 2002). These studies also led to recognition of several styles of MTDs in the lowermost Miocene Whakataki Formation: (1) either mostly reworking the pelagic unit (Chanier and Ferrière 1991; the Pahaoa and Flat Point olistostromes) or the intermediary to detrital units from the Upper Cretaceous to Oligocene series (Neef 1995; Delteil et al. 2006; Down 2016; the Suicide Point and Mataikona breccias); (2) representing single or several events of mass wasting (Chanier and Ferrière 1991; the Flat Point olistostrome vs the Pahaoa olistostromes); (3) comprising varying interactions with the contemporaneously developing Whakataki turbidites (*e.g.,* Chanier and Ferrière 1991; the interbedded Flat Point olistostrome).

2.4. Castlepoint trench-slope basin

The study area is located on the western limb of the Castlepoint trench-slope basin, a newly identified sub-basin to the East Coast Basin domain. Partially emergent at present day, the Castlepoint trench-slope basin is a narrow (currently two to four kilometers wide at the outcrop, possibly up to 15-20 kilometers depending on the exact location of its outboard basin boarder), elongated (~120 kilometers long) and trench-parallel (NE-SW) intra-slope basin of the Hikurangi subduction wedge (Figure 2). Its landward margin is controlled by the seaward-directed Flat Point-Whakataki Fault complex (Figure 2; Figure 5) which transported pre-Miocene strata on its back (*i.e.,* the Glenburn Nappe in Chanier and Ferrière 1991) thrusting over the contemporaneously developing syn-subduction strata (*e.g.,* lowermost Miocene Whakataki Formation) (Figure 2; Figure 5; Figure 6). The Flat Point-Whakataki Fault complex and its associated thrust ridge formed and still forms its inboard basin-bounding structure, separating it from the 'Whareama trench-slope basin' to the south and the 'Akitio trench-slope basin' to the north (Figure 2). The location of its seaward margin remains uncertain however, being underwater. The Turnagain Fault could be a candidate (see Figure 2 and 6 of Malie et al. 2017).

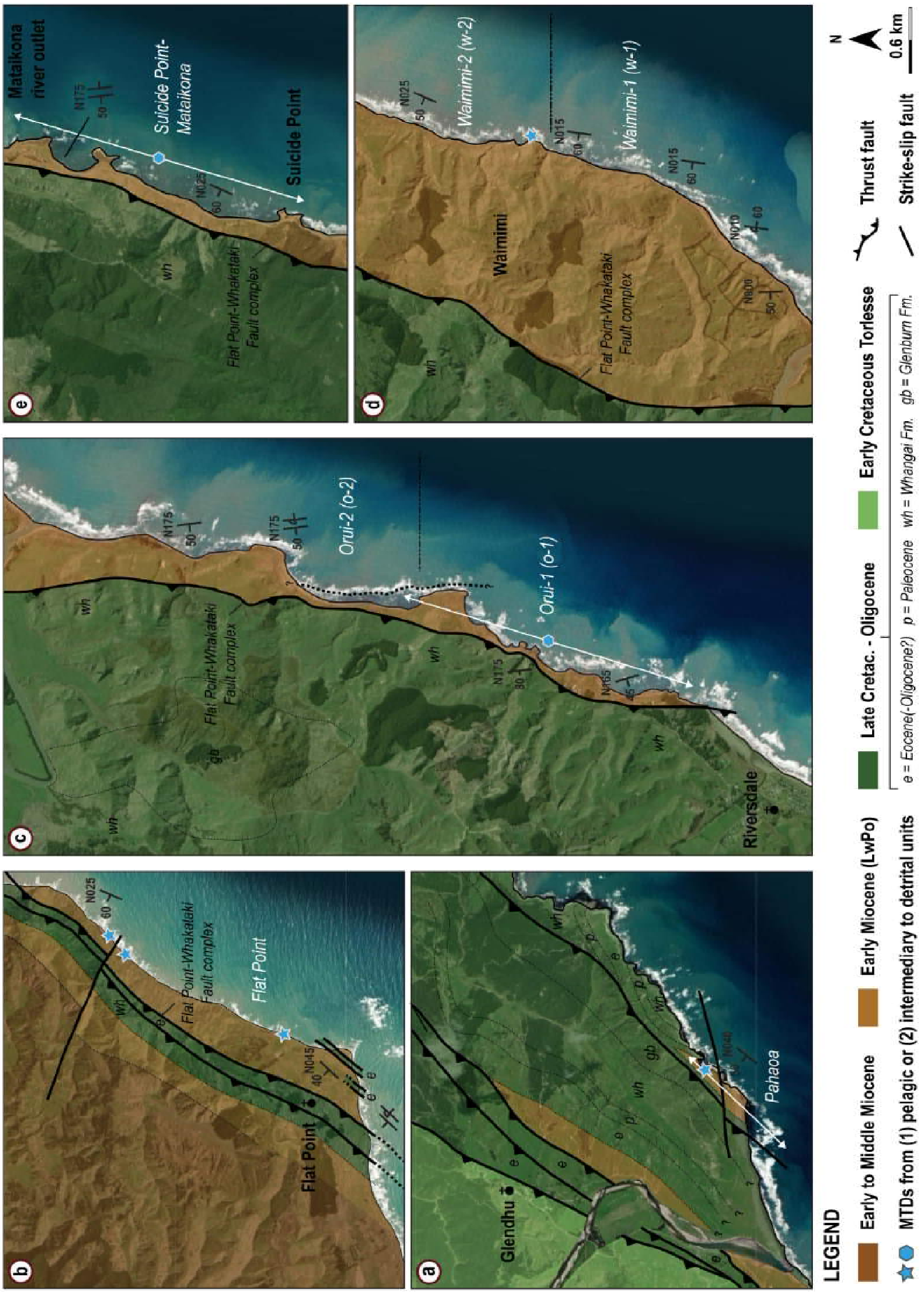

Figure 5: Satellite maps from World Imagery (ESRI), and onshore geological maps adapted from Chanier (1991) and 1:250 000 Geological Map of New Zealand (QMAP) of Wairarapa (https://www.gns.cri.nz/)) for each of the lowermost Miocene [NZ stage: late Waitakian-Otaian] coastal sections = (a): Pahaoa section, (b): Flat Point section, (c): Orui sections, (d): Waimimi sections and (e): Suicide Point-Mataikona section. Location (symbol) and extent (arrows, if applicable) of the mass-transport deposits that essentially rework pre-subduction margin series in each section localities. Due to outcrop extent and contrasting stratigraphic features, the Orui (o) and Waimimi (w) outcrops were both subdivided into two sections, corresponding to the southern (o-1, w-1) and northern (o-2, w-2) exposures.

Accepted Manuscript version. Published Journal Article version available online, published by Elsevier in Marine and Petroleum Geology Journal: https://doi.org/10.1016/j.marpetgeo.2023.106191

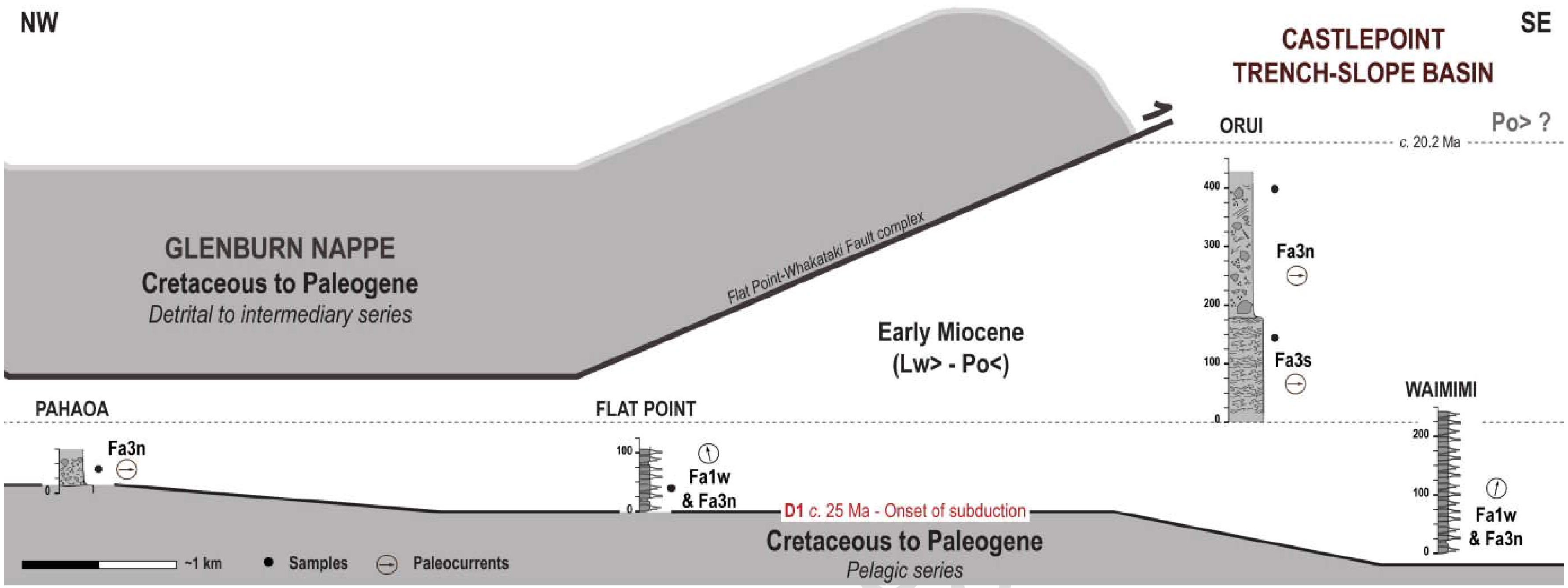

Figure 6: NW-SE correlations of the lowermost Miocene [NZ stage: late Waitakian-Otaian] Whakataki Formation gravity-driven deposits. Sedimentological vertical sections were collected along the Castlepoint trench-slope basin, to the east of its landward basin-bounding structure (*i.e.,* Glenburn Nappe) controlled by the underlying seaward-directed Flat Point-Whakataki Fault complex. The template used follows the one that was previously built by (Bailleul et al. 2013) for the Akitio trench-slope basin. Fa1w – refers to channel-levee system; Fa3n – to mass-wasting system mostly reworking pre-subduction margin series; Fa3s – to mass-wasting system reworking syn-subduction margin series. Location of coastal sections shown on Figure 5 : (a): Pahaoa section, (b): Flat Point section, (c): Orui sections, (d): Waimimi sections. See Appendix 3 for sampling details.

3. DATA AND METHODS

This outcrop-based study examines the lowermost Miocene Whakataki Formation cropping out in the Castlepoint trench-slope basin of the southern coastal ranges of the North Island. In this context, three field campaigns (2018, 2019, 2020) were carried out acquiring high-resolution sedimentological, structural and photogrammetric data along 80 kilometers of the coast. Five main localities were analyzed, three of which were previously partly described by Chanier and Ferrière (1991) (Pahaoa and Flat Point sections; Figure 2a, b; Figure 5a, b; Figure 6), Neef (1995), Delteil et al. (2006) and Down (2016) (Suicide Point-Mataikona section; Figure 2e; Figure 5e; Figure 6); and two of which remained undescribed until now (14 kilometers of coastline to the north of Riversdale, Orui and Waimimi sections; Figure 2c, d; Figure 5c, d; Figure 6).

3.1. Outcrop data

Field mapping data were recorded with a Trimble ® TDC100 and integrated using ArcGIS software tools. Detailed sedimentary sections were measured at bed scale (1:50) to characterize the Whakataki Formation turbidites in this area, totaling 872 meters and summarized in Table 1, Figure 7, Figure 8 and Figure 9 and Figure 10. A dedicated diagnostic feature template was used to thoroughly describe each Whakataki Formation MTD occurrence in a standardized manner and completed using abundance charts for visual percentage (Terry and Chilingar 1955) (see pie charts in Figure 9 and Figure 11). The combination of the two allowed us to create a synthetic sedimentary section for the Orui locality presented in Figure 11. For the previously studied Pahaoa and Suicide Point-Mataikona localities, an overview of their deposits is provided on Figure 12.

A total of 123 structural measurements (*e.g.,* ductile deformation analysis in both the MTDs and turbidites) as well as 481 paleocurrent indicators (measured from three-dimensional ripples, primary current lineations and sole marks within and at base of turbidite beds) were collected. The measurements were corrected using the geomagnetic models from GNS Science New Zealand and restored to pre-tilt position after back-tilting of bedding planes to initial horizontal position (assuming cylindrical folding). They are presented in context of their outcrops in Figure 8, Figure 9, Figure 10, Figure 13, Appendix 1 and Appendix 2.

Fieldwork data were complemented by micropaleontological analysis (foraminiferal content) conducted by GNS Science New Zealand to determine the age of the sedimentary units and related depositional paleobathymetries (Figure 6; Appendix 3). Samples were collected in the Orui and Waimimi sections to supplement the Fossil Record Electronic Database FRED (https://fred.org.nz/) (Clowes et al. 2021) since these areas currently appear as Quaternary beach deposits on the 1:250 000 Geological Map of New Zealand (QMAP) of Wairarapa (https://www.gns.cri.nz/). For the Pahaoa, Flat Point and Suicide Point-Mataikona sections, we referred to previously collected samples, either available in FRED or in Chanier (1991). Thin-section analysis was performed on one of the samples in order to characterize the origin, but also the age of the associated rock on the basis of the micropaleontological content (Appendix 4).

High-resolution images were taken with a DJI Phantom 4 Pro drone (Figure 8; Figure 9; Figure 11; Figure 13). Georeferenced outcrop models in the form of triangulated meshes textured with the photographs were then created (Figure 8; Appendix 1; Appendix 2) to display the stratigraphic architectures and help the characterization of the facies organization.

3.2. Lithofacies and facies associations

A lithofacies scheme was developed for the five localities. Seven lithofacies were identified, based upon their dominant lithology and primary sedimentary features, and interpreted in terms of processes (summarized in Table 1 and represented in Figure 7).

Together, they form three facies associations (**Fa1w, Fa3n, Fa3s**) that are characterized by distinct architectures, lithofacies organization and depositional systems (Table 2). In this study, we leveraged on and complemented the initial trench-slope basin nomenclature that was defined by Bailleul et al. (2007) and Bailleul et al. (2013), and where **Fa1** are associated to turbidite systems and **Fa3** to mass-wasting deposits.

3.3. Ductile deformation analysis

In this tectonically active setting, particular attention was paid to the tectonic or sedimentary origin of the folds affecting the same poorly lithified material (facies association **Fa1w**). As previously highlighted by Waldron and Gagnon (2011), whether the driving forces that led to soft-sediment deformation (*sensu* Maltman 1984) are largely (1) “superficial, gravity-driven” or (2) “rooted, tectonic” processes remains a challenging question, and more particularly since they believe that a geologist examining the deformed rocks is unlikely to be able to tell the difference from outcrop evidences.

In this outcrop-based study however, the distribution of the fold axis and axial planes affecting the same poorly lithified material (facies association **Fa1w**) provided a first recognition criterion, either revealing

Accepted Manuscript version. Published Journal Article version available online, published by Elsevier in Marine and Petroleum Geology Journal: https://doi.org/10.1016/j.marpetgeo.2023.106191

(1) a scatter of data, as sometimes observed in slump-related folds (Alsop and Weinberger 2020) with however a preferential dip direction, or (2) consistent patterns, similar to that of the Early Miocene regional paleostress field. The stratigraphic position(s) of the soft-sediment deformation has then allowed to reconcile these first observations with the larger geological settings. Clues for deciphering their dominant driving forces were therefore gained by combining insights from the ductile deformation analysis, the stratigraphic position of the related soft-sediment deformation and the regional tectonics. The extent (kilometers) of the outcrop exposures were critical, not only providing distorted and partial views of the fold profiles, but instead allowing a consistent mapping of the deformation.

4. LOWERMOST MIOCENE WHAKATAKI FORMATION

4.1. Turbidites

4.1.1. Fa1w: Axial channel-levee system

Observations

Fa1w is characterized by (1) broadly lenticular, commonly very-thick bedded (average two to three meters), fine-grained clean sandstones capped with well-developed mudstones (**HDTC**), interbedded with (2) relatively continuous, flat and on average thin-bedded, fine sandstones and mudstones (**LDTC**) (Table 1; Table 2; Figure 7). The transition between these two lithofacies regularly shows angular relationships (*e.g.,* downlaps, erosional truncations) (Figure 8a, a1, a3, a4; Figure 9a).

The thicker beds (**HDTC**) are frequently amalgamated (Figure 8a2, a3, b2, b4, c). Their concave up and erosional bases are usually coarse-grained, with mud clasts and sometimes trough cross-stratifications (Figure 7). They truncate the underlying thin-bedded strata (**LDTC**) with broad, metric, rarely decametric incisions, which can be traced across several tens of meters along the outcrop (Figure 8a1, a3, b1, b4). The percentage of bed amalgamation seems to proportionally increase with the size of the incision (Figure 8a2, a3); for example, the largest incision (up to 30 meters deep) records at least six distinct, semi-amalgamated channels. Most sandstone beds include several grain-size breaks, well-developed dewatering or soft sedimentation deformation structures, and frequently end with thick intervals of faint laminations, wispy convolute laminations and patchy silt pseudonodules in very fine-grained sandstones to siltstones (Figure 7; Figure 8c). The mud caps are particularly thick and regularly appear to fill the remaining lenticular relief (Figure 8a1, a4, b1, b4).

Accepted Manuscript version. Published Journal Article version available online, published by Elsevier in Marine and Petroleum Geology Journal: https://doi.org/10.1016/j.marpetgeo.2023.106191

The associated thinner beds (**LDTC**) are commonly organized in packages about ten meters thick (Figure 8a1), occasionally several tens of metres thick (Figure 8b1). They are truncated at the top by the thicker sandstone beds (**HDTC**) (Figure 8a3, b1) and can show wedging geometries with low-angle downlap terminations onto the underlying mudstone cap of the thicker sandstone beds (**HDTC**) or within the interval itself (**LDTC**) (Figure 8a1, b1; Figure 9a; Appendix 1; Appendix 2). The structured sandstone beds are generally thin-bedded and can show disseminated fine to very fine plant debris. Occasional occurrences of medium-bedded intervals are present and tend to have sole marks, such as flute casts.

Paleocurrent measurements (with bedding restored to horizontal position) show consistent near-orthogonal relationship between the thicker (**HDTC**) and thinner sandstone beds (**LDTC**) and indicate currents that are dominantly northward-directed (Figure 8; Appendix 1; Appendix 2).

Shear zones are frequently observed in **Fa1w**, generally comprising shear and fault planes either resulting in flexural-slip features (Figure 8b, b3) or combined with remobilized (**SL-b**) and or contorted (**SL-a**) strata (Figure 8b1, b4; Figure 10). This dominantly ductile soft-sediment deformation affects both the **HDTC** and **LDTC** intervals, and sometimes results in localized repetition of the series (Figure 8b; Figure 10; Appendix 2). The associated folds are sometimes upright, mostly inclined to recumbent and generally hold meters to several meters' wavelength. They are characteristically NE-SW directed with their hinges preferentially dipping towards the east (Figure 10).

Finally, in three instances, very thick-bedded (up to three meters), disorganized, polymict and matrix-supported conglomerates (**DF**) were observed to interrupt these series (two of them illustrated on the logs of Figure 9). Their base is sharp and erosive into the mudstone caps, whereas their rugose topography is usually overlain by the **HDTC** sandstones that locally rework the conglomeratic content at their base or incorporate some of the outsized clasts (Figure 9b). These different deposits are discussed in detail below (see Section 4.2.1, facies association **Fa3n**).

At Waimimi, **Fa1w** reaches up to 270 meters in thickness to the south and over 400 meters to the north, and typically shows several kilometers of lateral continuity (Table 2; Figure 5d; Figure 6; Figure 8; Appendix 1; Appendix 2). Once corrected for post-depositional deformation, the thicker beds (**HDTC**) display a general dispersion of current directions from the SW to the N at Waimimi-1 whereas they indicate a fairly consistent NE direction at Waimimi-2. The thinner beds (**LDTC**) are preferentially directed to the NNW (Figure 8; Appendix 1; Appendix 2).

Accepted Manuscript version. Published Journal Article version available online, published by Elsevier in Marine and Petroleum Geology Journal: https://doi.org/10.1016/j.marpetgeo.2023.106191

Figure 7: Representative photographs of the lithofacies summarized in Table 1 and encountered at the Pahaoa, Flat Point, Orui, Waimimi and Suicide Point-Mataikona localities. See Table 1 for the description of the lithofacies codes.

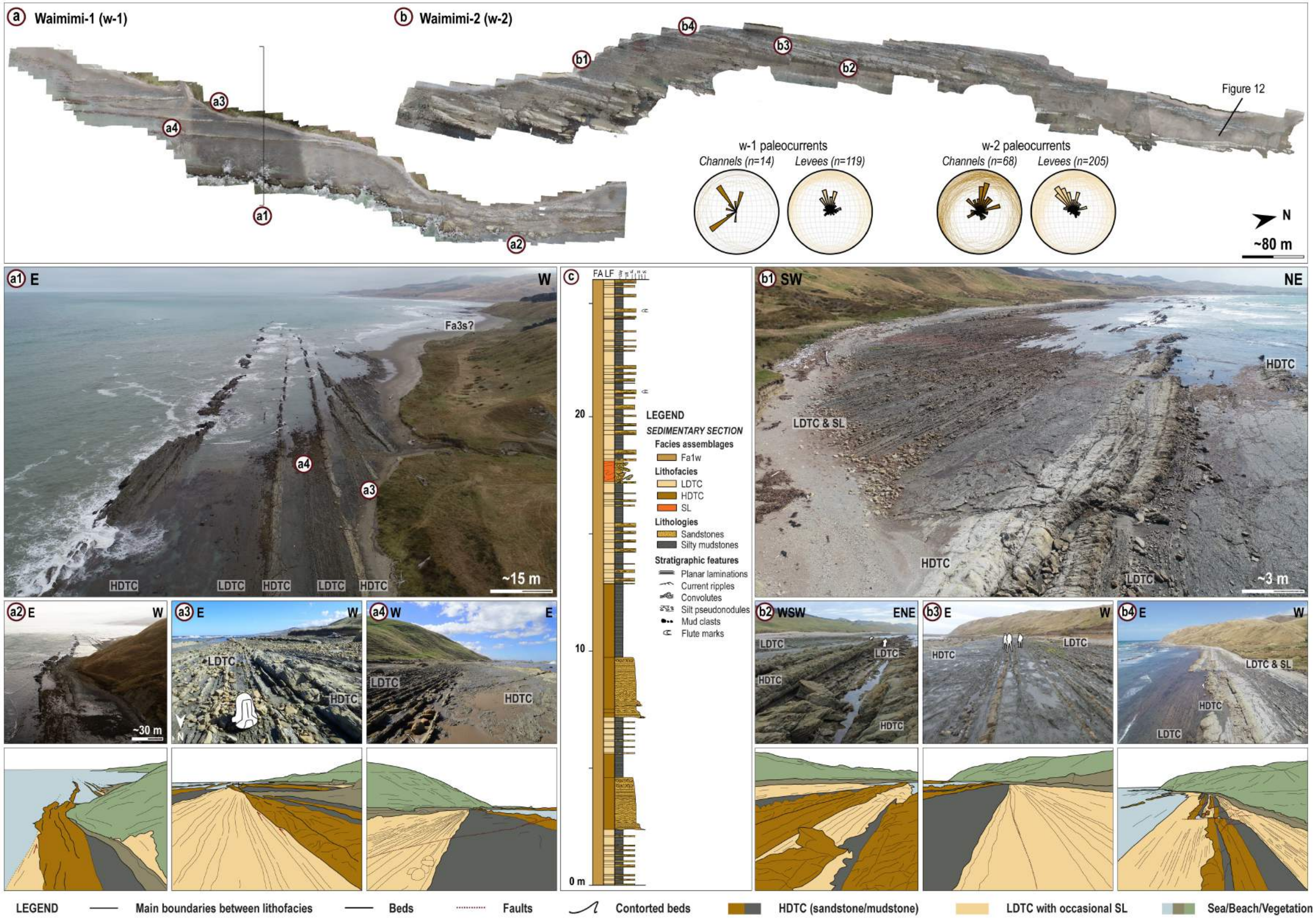

Figure 8: 3D outcrop models, paleocurrent analysis as well as detailed photo interpretations of the lowermost Miocene channel-levee system (Fa1w) observed at Waimimi. This coastal outcrop is divided into two sections, namely section w-1 to the south and section w-2 to the north. The letters (a) and (b) respectively refer to some of the architectural elements that characterize the w-1 and w-2 sections. The letter (c) captures a sedimentary section that synthetises the stratigraphic pattern of the channel-levee system. See Table 1 for the description of the lithofacies codes (HDTC, LDTC, SL) and Table 2 for the facies association codes. See Appendix 1 and Appendix 2 for enlarged views of the Waimimi outcrop models, respectively the southern part (w-1) and the northern part (w-2).

At Flat Point, **Fa1w** is approximatively one hundred meters thick, cropping out along several kilometers of coastline (Table 2; Figure 9). It conformably overlies the Eocene-Oligocene pre-subduction margin series and is overthrusted by the seaward-directed Flat Point-Whakataki Fault complex (Figure 2b; Figure 5b; Figure 6). At Flat Point, the series includes a higher proportion of **HDTC** intervals, which are interbedded with smaller **LTDC** intervals that generally comprise sandier and thicker sandstone beds to that of Waimimi. The internal architecture is also more complex, displaying numerous sharp erosional truncations, concave-up geometries and downlap terminations (Figure 9a). The paleocurrents are dominantly directed to the NW (Figure 9a).

Interpretations

We interpret **Fa1w** to represent the development of an aggradational (minimum 230 meters thick at Waimimi) and laterally extensive (several tens of kilometers axially to the basin) turbidite-rich channel-levee complex system (Mutti and Normark 1991; Galloway 1998; Sprague et al. 2005; Kane and Hodgson 2011), which ran parallel to the trench-oriented basin bounding structures. The broadly lenticular, sandstone- to mudstone-rich deposits (**HDTC**) result from confined, waning turbidity currents and characterize the infilling of channel-forms, whereas the thinner-bedded heterolithic intervals represent the relatively unconfined portion of flows spilling over the channels and forming their levee-overbank deposits (**LDTC, SL-a, SL-b**) (Mutti and Normark 1991; Galloway 1998; Kane and Hodgson 2011).

The channel fills (**HDTC**) characteristically provide greater preservation of the waning cycles and hold rather thin channel fills in comparison to their widths (Figure 8) (Mutti and Normark 1991; Galloway 1998; Hodgson et al. 2016). Their internal organization is complex and record multiple cycles of sub-horizontal channel-fills (*e.g.,* recurrent grain-size breaks), largely dominated by fine-grained sedimentation with an overall evolution from traction- through suspension fall out- to suspension-dominated depositions (*e.g.,* Bouma 1962; Stow and Shanmugam 1980). We interpret these infills to result from a succession of (rather than a single) turbidity flow events.

At both Flat Point and Waimimi, these channels are typically underfilled ending with very thick-bedded mudstone caps (likely substantially compacted already (Jones 1944)), reflecting their recurring abandonment, and possibly avulsion (Galloway 1998; Sylvester et al. 2011). Unfilled reliefs tend to strongly impact the location and morphology of the next channel, thereby favoring the development of organized stacking patterns with negligible channel offset such as the ones observed here (Figure 8) (Posamentier and Kolla 2003; McHargue et al. 2011).

The recurrent packages of thin-bedded turbidites (**LDTC**) are attributed to the levee-overbank deposits (Kane and Hodgson 2011; McArthur et al. 2016) needed for aggradation from one channel to another (Mutti and Normark 1991). Their generally uniform to progressively swinging paleocurrent directions (Figure 8), their sedimentary structures characteristics of simple waning flows (*i.e.,* partial Bouma sequences), their broad wedge geometry, varying thicknesses and downlap terminations all suggest deposition from unconfined overbank flows (Kane and Hodgson 2011).

The near-orthogonal relationships observed in the paleocurrent directions, well-expressed in Waimimi-2, are consistent with a turbidite channel-levee system and suggest channelized flows, though sparse, generally to the north along with longitudinal flows alternatively to the NW and NE at Waimimi. Although the micropaleontology analysis indicates that deposition occurred at deep bathyal depths (>800 meters) during the earliest Miocene, late Waitakian to Otaian (Aquitanian to Early Burdigalian, 23.03 – 18.7 Ma) (Appendix 3), the presence of terrigenous organic material highlights that the turbidity flows most likely initiated from shallow marine environments that were connected to a vegetated hinterland (Kuenen 1964).

Contemporaneous turbidites similar to these (**LDTC**, disputably 750 to 1500 meters thick) have been described further north, to the north of Castlepoint (Figure 2). They were interpreted to result from medial and distal levee-overbank setting with longitudinal flow directions to the NNE (Field 2005), supplied from a sediment source close to the continent (*i.e.,* vegetated hinterland and nearshore/shelf environments) (Sloss et al. 2021; Griffin et al. 2022). The Flat Point and Waimimi **Fa1w** deposits could therefore represent relatively proximal expressions of such a channel-levee complex system, either sourced from one or multiple entry points, advancing and feeding the more distal deposits to the north.

Finally, we attribute the compressional features affecting the poorly lithified **Fa1w** deposits to result from post-depositional tectonic overprint related to the earliest Miocene period of regional NE-SW seaward thrusting (Chanier and Ferrière 1991). Although local gravity-driven slope instabilities are common in levee-overbank settings due to oversteepening (Posamentier and Walker 2006), these structures were observed to mutually affect the channel and levee-overbank settings, and also provide incoherent paleoslope direction to those of the related levee-overbank (Figure 10).

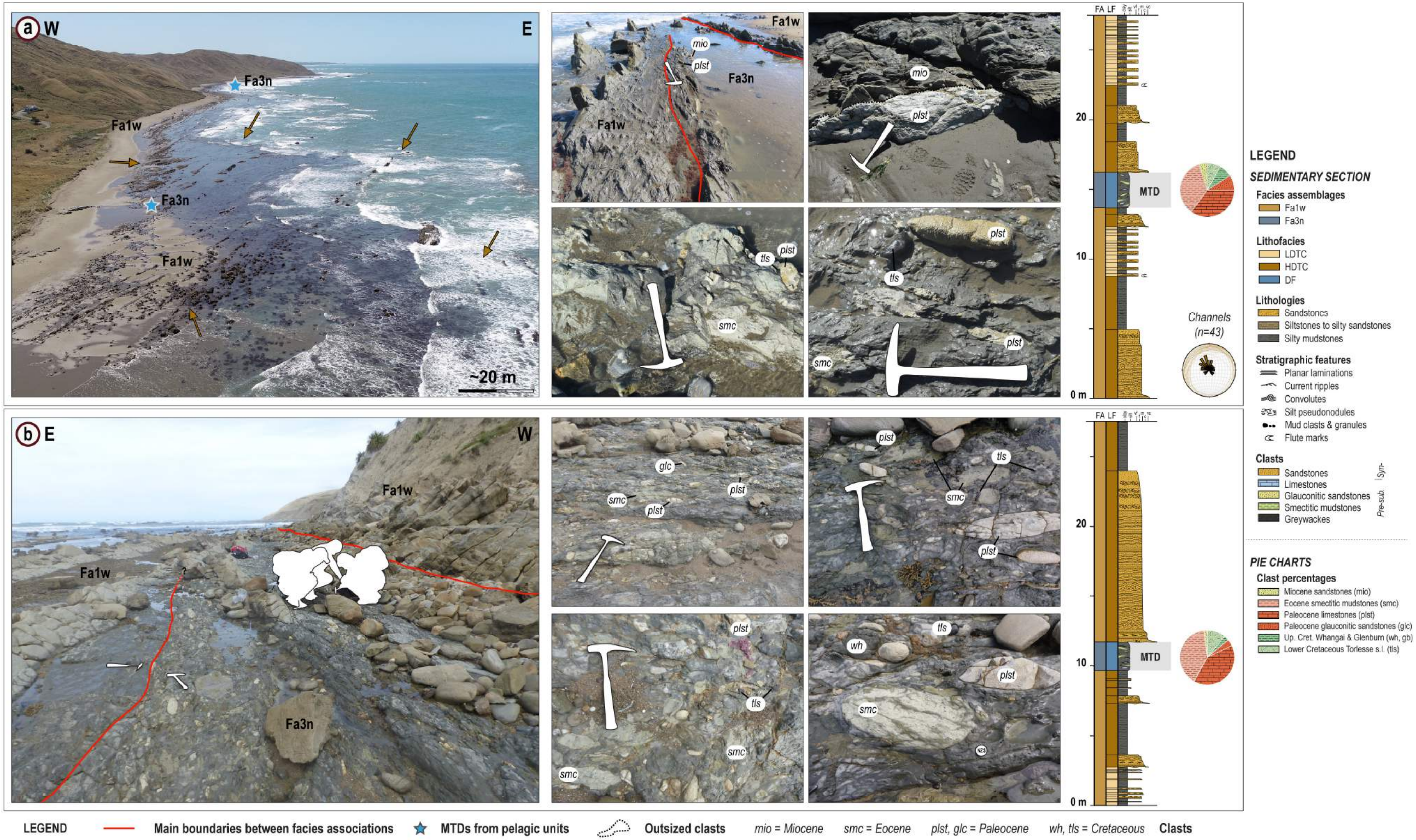

Figure 9: (a): Flat Point and (b): Waimimi mass-transport deposits (MTDs), interpreted to result from the frontal erosion of thrust sheets (Fa3n) developed in the pelagic units of the Hikurangi margin pre-subduction series and interrupting the lowermost Miocene channel-levee system (Fa1w). Detailed views of the MTDs and their lithoclast content. The sedimentary sections are composite sections, capturing their stratigraphic relationship with the coeval channel-levee systems. The pie charts provide insights as to the nature and associated proportions of each lithoclast style. mio = sandstones (*e.g.,* Fa1w); smc = smectitic mudstones; plst = whitish sub-micritic limestones; glc = glauconitic sandstones; wh = calcareous or siliceous mudstones; tls = greywackes. The yellow-brown arrows on the top-left picture highlight the complex internal architecture of Fa1w. See Table 2 for the description of the facies association codes.

Accepted Manuscript version. Published Journal Article version available online, published by Elsevier in Marine and Petroleum Geology Journal: https://doi.org/10.1016/j.marpetgeo.2023.106191

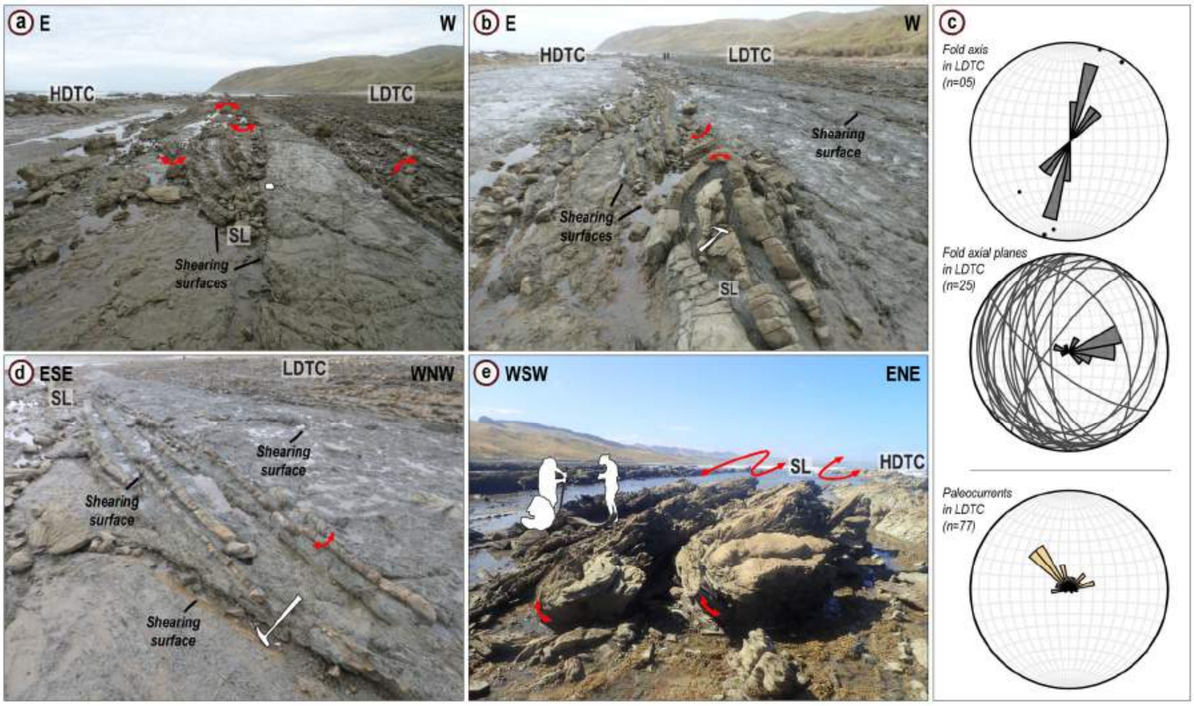

Figure 10: (a, b, d, e): Soft-sediment deformation (SL) recorded in the poorly lithified sediments of the Waimimi channel-levee system (Fa1w), interchangeably affecting the channel (HDTC) and levee-overbank (LDTC) settings. (c): Stereoplots (Schmidt, lower hemisphere) after back-tilting of bedding planes to initial horizontal position (assuming cylindrical folding) highlight the fold axis, axial planes and paleocurrent directions recorded in the levee-overbank settings presented here. Fold measurements were taken in the deformed zone (SL on pictures a, b, d and e) whereas the paleocurrents were taken in the structured intervals from the upper, undeformed zone (LDTC on pictures a, b and d). See Table 1 for the description of the lithofacies codes (HDTC, LDTC, SL)

4.2. Mass-transport deposits

4.2.1. Fa3n: Reworked pre-subduction series

<u>*General observations*</u>

Facies association **Fa3n** is characterized by disorganized, polymict and matrix-supported conglomerates (**DF, MF**) that rework randomly distributed pebble- to boulder-grade and outsized (deci- to pluri-decametric) extraformational lithoclasts derived from the pre-subduction margin series (Table 1; Table 2; Figure 7; Figure 9; Figure 11; Figure 12). Intraformational lithoclasts from the contemporaneously developing syn-subduction strata (*i.e.,* lowermost Miocene Whakataki Formation) were also sporadically observed. Clasts are supported by a light grey, silty mudstone matrix, which can locally show a higher siltstone content, as observed at Pahaoa (Chanier and Ferrière 1991) or at Orui (Figure 11c).

General interpretations

We interpret **Fa3n** to result from slope failure and mass-wasting processes that destabilized and reworked a paleogeographic domain(s) or structural unit(s) dominated by pre-subduction margin strata. The resulting deposits are therefore interpreted to represent mass-transport deposits (MTDs). They were likely produced by cohesive flows (*sensu* Mulder and Alexander 2001). The foraminiferal analyses of their matrix content indicate that deposition here occurred at minimum in middle bathyal (>800 meters) or possibly lower bathyal water depths (>1000 meters) during the earliest Miocene, late Waitakian to Otaian (Aquitanian to Early Burdigalian, 23.03 – 18.7 Ma) (Appendix 3). The contemporaneous onset of subduction and initial structural development of the subduction wedge resulted in the intense deformation of the passive margin, with the seaward emplacement of a succession of thrust sheets (Figure 4) (Chanier and Ferrière 1991; Rait et al. 1991). This, in turn, subaqueously exposed the rocks from the older pre-subduction substratum, ready to be reworked and incorporated into the subsequent mass-wasting processes. We therefore interpret **Fa3n** to derive from advancing thrust sheets (*sensu* Festa et al. 2010 and references therein).

In the study area, despite common characteristics such as the dominant lithology (*e.g.,* conglomerate), nature of the matrix (*e.g.,* silty mudstone) and of the clasts (*e.g.,* pre-subduction), significant differences exist, both in terms of their morphometric characteristics (*e.g.* size, extent) and their lithoclast content (*e.g.,* grade, roundness, age, detrital or pelagic origin). We here use the lithoclast nature (pre-subduction) and origin (thrust sheet unit) as a dividing criterion to further characterize the **Fa3n** MTDs and their source areas (Nemec and Steel, 1984). As a result, we identified two main recurrent yet distinct styles within the **Fa3n** facies association. These two styles are detailed below.

4.2.1.1. Reworking of pelagic units

Observations

The first style of **Fa3n** is encountered at Pahaoa (Figure 5a; Figure 12a), Flat Point (Figure 5b; Figure 9a) and Waimimi (Figure 5d; Figure 9b; Appendix 2).

In this first style (Table 2), the associated conglomerates comprise ~50 to 80% matrix content, with chaotically distributed lithoclasts (**DF**). They mostly (>80%) consist of sub-angular to sub-rounded pebbles to boulders of Paleocene limestones (*i.e.,* white micritic Kaiwhata limestones) and light green

Accepted Manuscript version. Published Journal Article version available online, published by Elsevier in Marine and Petroleum Geology Journal: https://doi.org/10.1016/j.marpetgeo.2023.106191

Eocene calcareous smectitic mudstones (Figure 9; Figure 12a). At Pahaoa, the clasts of Paleocene rocks are frequently several meters long (Figure 12a). Both characteristically present elongated, lenticular, sometimes sigmoidal shapes (Figure 9; Figure 12a). For the Eocene strata however, the very flat shapes are systematically oriented parallel to the matrix bedding.

For the remainder of the pre-subduction clasts, their content varies slightly at the different locations (Figure 9; Figure 12); it generally includes Lower Cretaceous strata, Upper Cretaceous calcareous sandstones (*i.e.,* Whangai Formation) and Uppermost Cretaceous to Paleocene glauconitic sandstones. The Lower Cretaceous lithoclasts mostly consist of (sub-)rounded granules and pebbles of greywackes (Figure 9), rarely of red cherts and lavas. At Pahaoa, a few scattered sub-angular boulders to outsized clasts of greywackes can also be found (Figure 12a). The Upper Cretaceous calcareous sandstone content is very scarce. Conversely, the Uppermost Cretaceous to Paleocene glauconitic sandstones are regularly present, either as sub-angular to sub-rounded pebble- to boulder-grade clasts or as contorted strata (Figure 12a). The syn-subduction content is rare; nevertheless, it typically occurs at the base of the conglomerate deposits as outsized clasts (decametric) of coherent to contorted thin-bedded turbidites of the Whakataki Formation.

At Pahaoa, this style of **Fa3n** is described by Chanier and Ferrière (1991). It can reach up to 40 meters in thickness and sporadically crops out over 900 meters along the coast (Table 2; Figure 5a), finishing its course under water. It conformably overlies (at least at the scale of the outcrop) the Paleocene to Eocene pelagic unit series (Figure 12a) and does not comprise one but a succession of coalescing (a few meters thick) conglomerates (**DF**) with a matrix greatly affected by complex syn-sedimentary folding (Chanier and Ferrière 1991) and mostly holding boulder-grade to outsized clasts. To the south, it is overlain by Whakataki Formation turbidites (**Fa1w**?) (Figure 5a) (Chanier 1991).

At Flat Point and Waimimi however, this style of **Fa3n** is only a few meters thick (up to three meters) and is interbedded with the **Fa1w** turbidites (see Section 4.1) (Table 2; Figure 9). Owing to the drone pictures, we were able to observe that the two **Fa3n** occurrences at Flat Point are not in the same stratigraphic position (Figure 9a) and as such do not correspond, as previously suggested by Chanier and Ferrière (1991), to a single and widespread conglomeratic episode but instead represent two distinctive episodes.

<u>*Interpretations*</u>

Owing to the extraformational lithoclasts that have lithological composition similar to that of the thrusted tectonic units, we interpret this first style of **Fa3n** to mainly result from the dismantlement of an

Accepted Manuscript version. Published Journal Article version available online, published by Elsevier in Marine and Petroleum Geology Journal: https://doi.org/10.1016/j.marpetgeo.2023.106191

advancing thrust sheet developed in the pelagic units of the Hikurangi margin pre-subduction series (-Figure 4B, pelagic unit) (Chanier and Ferrière 1989; Chanier and Ferrière 1991). Although discontinuous, the distribution of the resulting deposits suggests that these pelagic units were consistently exposed to submarine erosion along the southern Hikurangi margin at the time.

The analysis of the syn-sedimentary deformation recorded in the deposits (see Chanier and Ferrière 1991) indicates that the failed material was transported downslope and subsequently deformed (*e.g.,* shearing structures, intrafolial folds) through mass-wasting processes (*e.g.* Festa et al. 2016) and also that the transport direction was to the E or NE. The rafted blocks of turbidites, recurrently found at the base of **Fa3n**, suggest basal interaction and substrate disruption from the overriding mass (Posamentier and Martinsen 2011; Sobiesiak et al. 2018).

The **Fa3n** deposits do not point toward an isolated catastrophic event but rather a series of semi-continuous mass-wasting events that were linked to the seaward emplacement of a thrust sheet (Chanier and Ferrière 1991), and which triggered successive debris flows (*sensu* Mulder and Cochonat 1996).

The deposits at Pahaoa would represent a relatively proximal expression of the failures, being coarse-grained, thick and coalescing in front of the propagating thrust sheet; whereas the Flat Point and Waimimi deposits would represent thinner, more distal incursions, occasionally reaching the Castlepoint trench-slope basin floor several kilometers to the east, and interacting with the contemporaneously developing turbidite system (**Fa1w**). The contrasting styles and thicknesses could result from (1) MTDs that thin away from their source towards the trench-slope basin center, (2) different magnitudes of mass-wasting events (*e.g.,* Watson et al. 2020), (3) similar sources but with contrasting catchment sizes (*e.g.,* Naranjo-Vesga et al. 2020), or (4) a preferential routing of the MTDs interacting with the turbidite system (*e.g.,* Pickering and Corregidor 2005; Ortiz-Karpf et al. 2017). A different timing of events could also be envisaged with a sustained period of mass-wasting (Pahaoa MTDs) occurring before the establishment of the turbidite system (Flat Point and Waimimi **Fa1w** turbidites), only then followed by some punctuated tectonic pulses that would episodically (but not necessarily always) produce MTDs locally seen to reach and interrupt the turbidite sedimentation taking place in the trench-slope basin (Flat Point and Waimimi MTDs). Detailed micropaleontological analyses are however required to ascertain such scenarios and along slope controls.

Although mass-wasting processes traditionally represent a continuum along slope, whereby one process can evolve into or trigger another (Stow 1986; Nemec 1990), the comparisons of the proximal and distal expressions of similar slope failures here indicate that the mass-wasting process did not

Accepted Manuscript version. Published Journal Article version available online, published by Elsevier in Marine and Petroleum Geology Journal: https://doi.org/10.1016/j.marpetgeo.2023.106191

change. This suggests very little to no flow transformation (Fisher 1983) that may be due to strongly coherent debris flows, typically extending back to their original failure (*sensu* Talling 2013).

Finally, at Pahaoa, the (sub-)rounded pebbles of Lower Cretaceous strata, constantly present in these **Fa3n** deposits, unlikely come from the underwater substratum and might instead result from direct erosion of the hinterland (*e.g.,* Bland et al. 2022) or reworking of the Upper Cretaceous conglomerates, comprising already fluvially-reworked greywackes (Chanier 1991; Chanier and Ferrière 1991).

4.2.1.2. Reworking of intermediary units

Observations

The second style of **Fa3n** is here described using the southern Orui locality as reference (Table 2; Figure 5c, the Orui-1 section (o-1); Figure 11).

The associated conglomerates are primarily distinguished by varying matrix content (Table 1; Figure 11c;). They frequently present more than 95% (**MF**); yet, are often interspersed by intervals with lesser matrix (~50%, **DF**) laterally and or vertically evolving into **MF**. The matrix characteristically shows compositional foliations. Only one instance was observed to virtually hold no matrix (**CF**).

Contrary to the previously described **Fa3n** style (see Section 4.2.1.1), these conglomerates show an upward evolution in the nature of their clast content (Figure 11c). The lithoclasts however remain randomly distributed.

In stratigraphic order, the basal conglomeratic units (here, MTDs 01 to 04) mostly (>75 to 90%) comprise pebbles to outsized clasts (deci- to decametric) of Paleocene limestones (sub-micritic equivalent to the white Kaiwhata limestones), Paleocene siltstones (*i.e.,* Waipawa Formation) and light green, red or black Eocene calcareous smectitic mudstones (Figure 11c, d6, d7, d8, d9). Both the Paleocene limestones and Eocene lithoclasts present elongated shapes, recurrently asymmetrical (both sinistral and dextral geometries), similar to that of the previously described **Fa3n** style. In the clast-rich intervals (**DF**), the Eocene calcareous smectitic mudstones are often intricately interbedded with the lowermost Miocene matrix and aligned along a N-S direction, parallel to bedding. These basal units also occasionally (>5 to 25%) reworked cobbles and outsized clasts of Uppermost Cretaceous to Paleocene glauconitic sandstones, as well as sporadically (2 to 15%) incorporated rafts (several tens of meters, *e.g.,* olistoliths) of Paleocene rocks, and more regularly of Upper Cretaceous siliceous rocks (*i.e.,* Whangai Formation) (Figure 11b, c). Syn-subduction clasts are only present in the first conglomeratic unit (~25%) as rafts of turbidite strata (Figure 11c).

Accepted Manuscript version. Published Journal Article version available online, published by Elsevier in Marine and Petroleum Geology Journal: https://doi.org/10.1016/j.marpetgeo.2023.106191

The following conglomeratic units (here, MTDs 05 to 08) mainly (~80%) consist of outsized clasts and rafts (several tens of meters) of Paleocene siltstones, Uppermost Cretaceous to Paleocene glauconitic sandstones and Upper Cretaceous limestones (sub-micritic equivalent to the Pithonellid-bearing limestones) (Figure 11c, d2, d4, d5; Appendix 4). They also generally incorporate Upper Cretaceous strata from the Whangai and more rarely Glenburn Formations, as well as interstratified very-thick intervals of Eocene calcareous smectitic mudstones.

The upper units (here, MTDs 09 and 10) are largely dominated by sub-angular pebbles to outsized clasts as well as rafts (several tens of meters) of Upper Cretaceous strata from both the Whangai (*e.g.,* siliceous mudstones with carbonate concretions) and Glenburn Formation (*e.g.,* conglomerates and sandstones) (Figure 11c, d1, d2). They also sporadically include sub-angular pebbles to boulders of Lower Cretaceous greywackes as well as outsized clasts (deci- to decametric) of Paleocene siltstones and Miocene turbidite strata (Figure 11c, d3).

Ductile and brittle-ductile deformation fabrics, such as asymmetrical boudinage and pseudo-sigma structures as well as intrafolial and rootless folds (*sensu* Festa et al. 2016), were commonly observed in the deposits (Figure 11).

At Orui, this style of **Fa3n** represents between 400 to 900 meters (lateral cumulative thickness) of successive MTD inputs, cropping out along ~four kilometers of coastline (Table 2; Figure 5c; Figure 11). Particularly, at the top of the series, the deposits are sometimes intercalated with pre-Miocene strata from the Coastal Block due to strike-slip faulting. The overall thickness estimate is therefore questionable; yet, remains particularly important (>400 meters). This style can be grouped into at least 10 distinct coalescing conglomeratic events, themselves comprising a series of internal events reworking material of similar nature (Figure 11c). Its basal surface is sharp and highly erosive (>20 meters) into the underlying **Fa3s** turbidites (see Section 4.2.2), and can be traced over one kilometer (Figure 11b). The outcrop conditions however hinder the exposure of its upper surface, which corresponds to the seaward-directed Flat Point-Whakataki Fault complex (Figure 2c; Figure 5c; Figure 11a, b).

To the north of the study area, between Suicide Point and Mataikona river outlet, a similar style of **Fa3n** crops out, roughly representing ~800 meters (cumulative thickness) of deposits, along more than three kilometers of coastline, also at the front of the Flat Point-Whakataki Fault complex (Table 2; Figure 5e; Figure 12b). The deposits were previously described by Neef (1995), Delteil et al. (2006) and Down (2016). Down (2016) identified two main events of conglomerate deposition separated by an episode of turbidite deposition and or folding (**Fa3s?**). The first (basal) conglomeratic unit, located close to the

Accepted Manuscript version. Published Journal Article version available online, published by Elsevier in Marine and Petroleum Geology Journal: https://doi.org/10.1016/j.marpetgeo.2023.106191

Mataikona river outlet (*i.e.,* Mataikona MTDs) (Figure 5e), would be monomict, either only reworking Upper Cretaceous material from the Whangai Formation (Neef 1995) or Upper Cretaceous to Eocene-Oligocene material from the Whangai, Kaiwhata, Wanstead and or Weber Formations (Down 2016). We here only focus on the second conglomeratic unit (~500 meters) (Figure 12b), located at and to the north of Suicide Point (*i.e.,* Suicide Point MTDs) (Figure 5e), characteristically holding similar deposits to those described in the Orui section (Figure 11).

Accepted Manuscript version. Published Journal Article version available online, published by Elsevier in Marine and Petroleum Geology Journal: https://doi.org/10.1016/j.marpetgeo.2023.106191

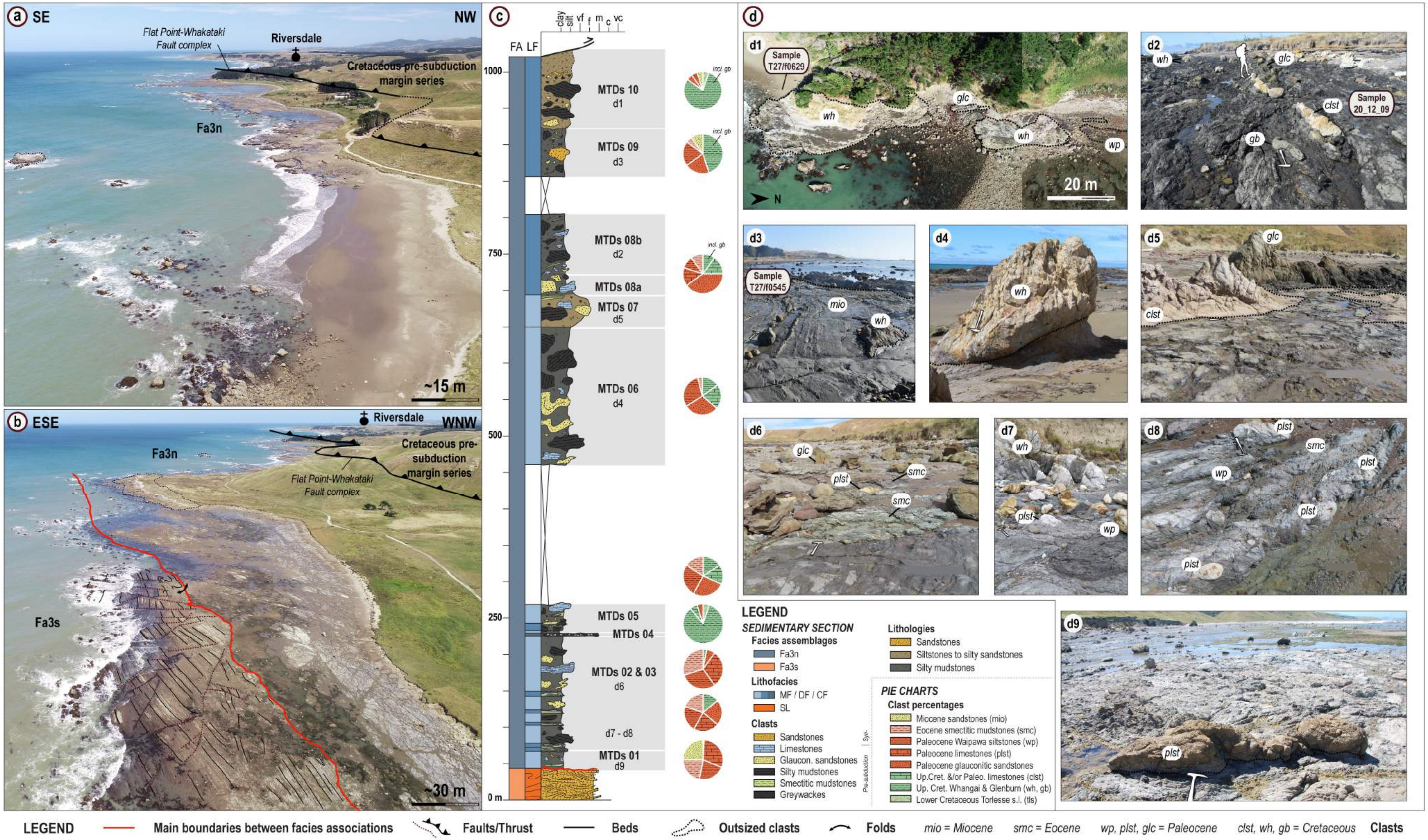

Figure 11: Orui mass-transport deposits (MTDs) resulting from the emplacement (Fa3s) and subsequent frontal denudation (Fa3n) of the Glenburn thrust sheet developed in the intermediary units of the Hikurangi margin pre-subduction series. (a, b): Drone views. (c): Composite sedimentary section capturing the main MTD styles, themselves comprising a series of internal MTDs reworking material of similar nature. The pie charts provide insights as to the nature and associated proportions of each lithoclast style. (d): Detailed views of the MTDs and their lithoclast content. mio = alternating sandstones and mudstones (*e.g.,* Fa1w); smc = smectitic mudstones; wp = organic-rich silty mudstones; plst = whitish sub-micritic limestones; glc = glauconitic sandstones; clst = pink-grey sub-micritic limestones; wh = calcareous or siliceous mudstones; gb = coarse detrital sedimentary rocks. See Table 2 for the description of the facies association codes.

Accepted Manuscript version. Published Journal Article version available online, published by Elsevier in Marine and Petroleum Geology Journal: https://doi.org/10.1016/j.marpetgeo.2023.106191

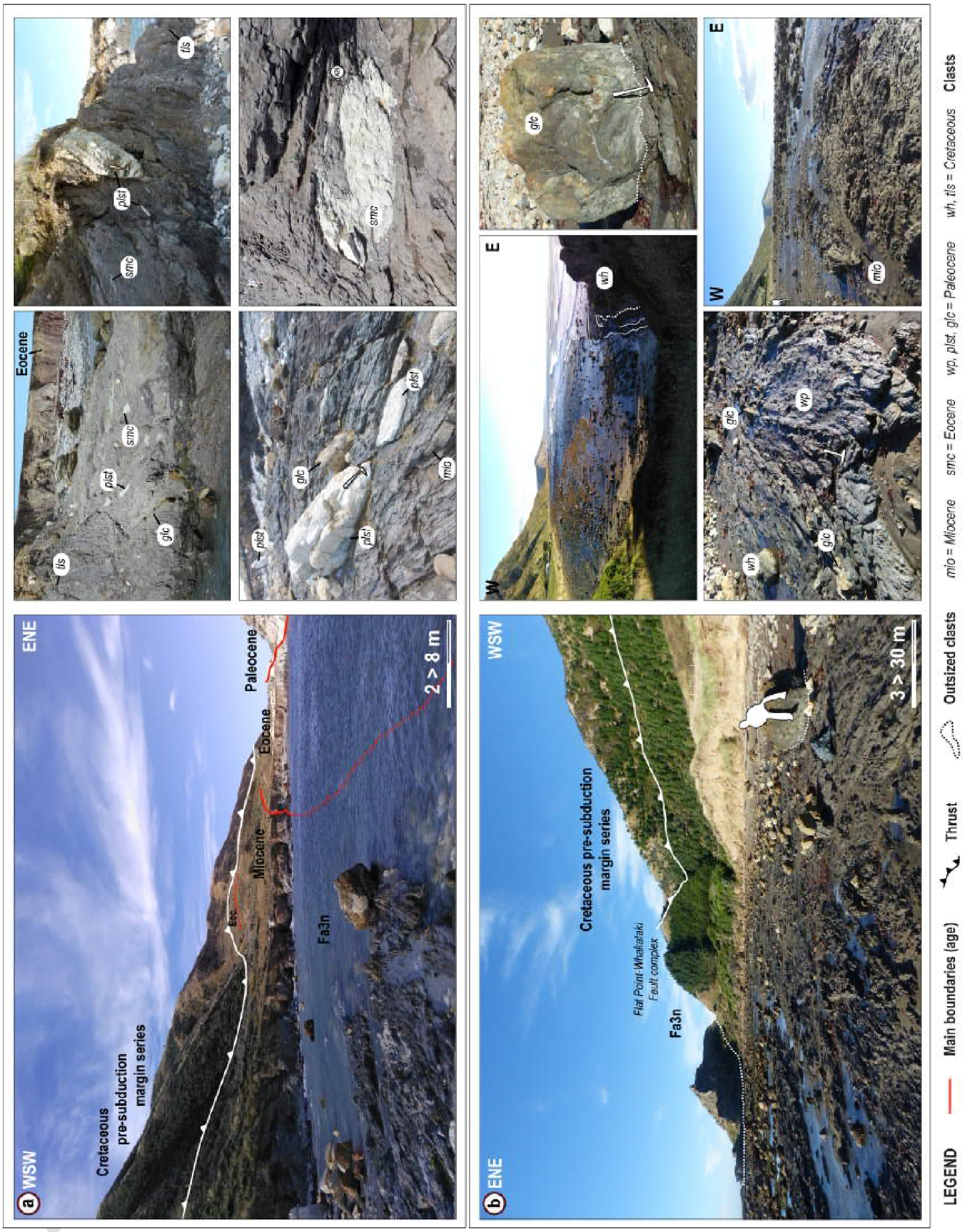

Figure 12: (a) Pahaoa and (b) Suicide Point mass-transport deposits (MTDs), resulting from the frontal denudation of thrust sheets (Fa3n) respectively developed in the pelagic units (first style of Fa3n) and intermediary units (second style of Fa3n) of the Hikurangi margin pre-subduction series. At Pahaoa (a), the Eocene strata (Eoc.) acted as *décollement* level. Present at the sole of the thrust sheet, these strata protected the underlying and overthrusted Pahaoa MTDs (see Section 5.1.1). Detailed views of the MTDs and their lithoclast content. mio = alternating sandstones and mudstones; smc = smectitic mudstones; wp = organic-rich silty mudstones; plst = whitish micritic limestones; glc = glauconitic sandstones; wh = calcareous or siliceous mudstones; tls = greywackes. See Table 2 for the description of the facies association codes.

Accepted Manuscript version. Published Journal Article version available online, published by Elsevier in Marine and Petroleum Geology Journal: https://doi.org/10.1016/j.marpetgeo.2023.106191

Interpretations

In this second style of **Fa3n**, the nature of the extraformational lithoclasts gradually evolves upward, recording progressive submarine exhumation and erosion of an advancing thrust sheet developed in the intermediary units of the pre-subduction series (Figure 4B, detrital and intermediary units; Figure 11; Figure 12b). Although, the basal units (corresponding to MTDs 01 to 04 at Orui) comprise a series of debris flows closely resembling the previously described **Fa3n** (see Section 4.2.1.1), the coeval presence of (1) Paleocene limestones that are sub-micritic equivalent to those in the pelagic unit and of (2) Waipawa strata both indicate remobilization of the intermediary (and not pelagic) units (Figure 4B). In the southern coastal ranges, the Glenburn Nappe, transported on the back of the seaward-directed Flat Point-Whakataki Fault complex, is a prime source candidate. Up to 1,500 meters thick, it records lateral facies transition from the detrital to intermediary poles eastwards (Chanier 1991), and directly overthrusts the thinner (typically 200 to 500 meters thick each) and underlying pelagic units (Figure 4) (Chanier and Ferrière 1989).

We interpret this second style of **Fa3n** to represent deposition from a semi-continuous, uninterrupted period of slope failure and mass-wasting processes, leading to the large-scale (~400 to 900 meters thick, several kilometers wide) remobilization and transport of the intermediary pre-subduction margin series, starting with the Paleocene-Eocene down to the Cretaceous strata, through consecutive debris flows and mudflows (*sensu* Folk 1954; Moncrieff 1989; Mulder and Cochonat 1996; Mulder and Alexander 2001).

Large mass-wasting events ascribed to advancing nappes typically present outsized clasts and rafts (*e.g.* Ogata et al. 2019), such as the ones described here. The disorganized clast fabric, average clast size (*i.e.,* outsized clasts) and shape (*i.e,* sub-angular) recorded throughout also suggest short travel distance from nearby source areas (Nemec and Steel 1984) and mobilization (*sensu* Iverson 1997). Notwithstanding succeeding advances of the nappe since then, making it even closer today (Figure 11), all the previously-stated elements strongly support MTDs that were already in close vicinity of the source, and at the front of the nappe (*sensu* Festa et al. 2010 and references therein).

Although also dating from the earliest Miocene (Appendix 3), these MTDs are not concurrent to the turbidite channel-levee complexes (**Fa1w**) documented at Flat Point as well as at Waimimi. Instead, they overlie it, thereby informing that this episode of erosion post-dates the one that affected the pelagic units and resulted in the emplacement of the first style of **Fa3n** (see Section 4.2.1.1).

The erosive character of the basal surface and the rafts of Miocene turbidites found at the base of the MTDs at Orui (*i.e.,* MTDs 01) both suggest basal ploughing and scouring leading to the incorporation of material from the overridden seafloor (*e.g.* Posamentier and Martinsen 2011; Sobiesiak et al. 2018). Conversely, lowermost Miocene clasts are next found in the upward part of the succession, and thus may indicate different processes, such as local ponding of contemporaneous turbidity currents (*e.g.,* Bull et al. 2009; Armitage et al. 2009), then subsequently remobilized during the next event of slope failure and mass wasting. Finally, the lithoclasts from the Lower Cretaceous strata only appear at the top of the series and may come from the direct erosion of the hinterland.

The foraminiferal analysis of sample T27/f02629, taken in the matrix content at the top of the series, informs that the Orui deposits date from the earliest Miocene and are restricted to the middle/late Waitakian to middle Otaian (Aquitanian, 23.2 – ca. 20.2 Ma) (Appendix 3). Between Suicide Point and Mataikona river outlet, although Delteil et al. (2006) proposed an Eocene age for the Mataikona MTDs, we here suggest, as highlighted by Neef (1995) and Down (2016), that owing to their stratigraphic relationships with the Whakataki Formation turbidites (**Fa1w** equivalent), both the Suicide Point and Mataikona MTDs were most likely earliest Miocene in age, and like the Orui deposits, linked to the nearby Flat Point-Whakataki Fault complex.

The absence of precise dating prevents us from providing a chronological order between the Orui and Suicide Point deposits. Yet, their characteristics inform that similar mass-wasting processes developed at the front of the Glenburn Nappe along the southern margin during that period. Among others, the 'reduced' thickness encountered at Suicide Point could be explained from (1) mass-wasting events of smaller magnitude, (2) a thinner Glenburn Nappe to the north and or (3) a more distal record of the deposits.

4.2.2. Fa3s: Remobilized syn-subduction series

<u>*Observations*</u>

Fa3s essentially comprises strata from the previously documented facies association **Fa1w** that is completely disorganized and remobilized (**SL-a, SL-b**) over several hundreds of meters vertically (Table 1; Table 2; Figure 7). Varying folding styles are observed including widely open upright folds, narrow recumbent folds as well as curvilinear and rootless folds (Figure 13). They are found across a large spectrum of scales, mostly displaying meters to tens of meters wavelength. The fold axis and hinge measurements reveal a rather scattered distribution; yet, they highlight a dominant N-S direction with

respect to present-day geography for the fold axis and a preferential eastward-verging plunge direction (Figure 13).

At Orui, **Fa3s** is about 300 meters thick and extends for several kilometers laterally. Its upper surface is erosive, NW-SE oriented (and so parallel to the dominant fold axis direction) and characterized by the following emplacement of **Fa3n** (see Section 4.2.1.2; Table 2; Figure 11b; Figure 13). At Orui, **Fa3s** ends with a contrasting style; although still locally including large-scale folding (**SL-a**) and sliding features (**SL-b**) (Figure 13c1, c2), the **Fa1w** strata seems largely undeformed in its upper ~65 meters (Figure 13a). **Fa3s** is also observed to the southernmost part of Waimimi (Figure 8a1). Between Suicide Point and Mataikona river outlet, **Fa3s** would correspond to the folded strata described in details by Down (2016), also typically overlain by **Fa3n**.

Interpretations

We interpret **Fa3s** to represent the large-scale soft-sediment deformation (several hundreds of meters, several kilometers) of the previously deposited and poorly lithified turbidites (**Fa1w**) (Maltman 1984). Notwithstanding a tectonic overprint, the variabilities encountered in fold geometries and orientations are not particularly coherent with the regional paleodirection of the main tectonic structures (NE-SW) (see Chanier and Ferrière 1991; Rait et al. 1991).

Accepted Manuscript version. Published Journal Article version available online, published by Elsevier in Marine and Petroleum Geology Journal: https://doi.org/10.1016/j.marpetgeo.2023.106191

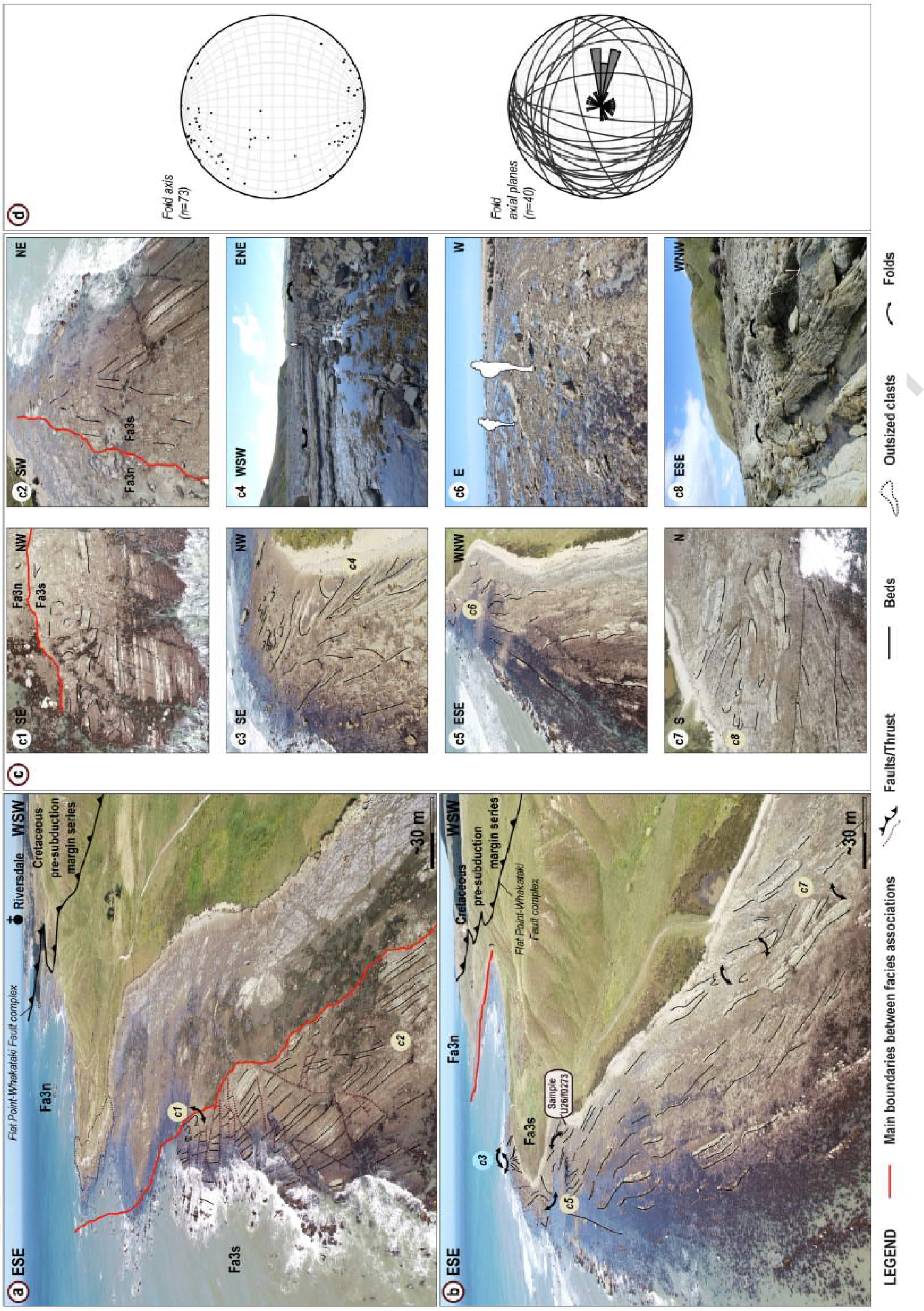

Figure 13: (a, b, c): Drone and detailed views of Fa3s. It is relatively undeformed in its upper part and overlain by Fa3n (c1, c2). Conversely, Fa3s is substantially deformed in its lower part (c3 to c8), whereby it is dominated by soft-sediment slumping (*sensu* Nardin et al. 1979) of the previously deposited, poorly lithified sediments of the channel-levee system (Fa1w). (d): Stereoplots (Schmidt, lower hemisphere) after back-tilting of bedding planes to initial horizontal position highlighting the fold axis and axial planes of the related slump-related folds. See Table 2 for the description of the facies association codes.

Accepted Manuscript version. Published Journal Article version available online, published by Elsevier in Marine and Petroleum Geology Journal: https://doi.org/10.1016/j.marpetgeo.2023.106191

Such observation therefore makes it difficult to envisage the contemporaneous tectonic deformation as a main driving process for the structures described here. Instead, their preferential N-S azimuthal direction and dip towards the east, both similar to that of the overlying deposits (**Fa3n**), as well as their stratigraphic position (underlying the second style of **Fa3n**) rather suggest that these **Fa3s** deposits were intrinsically related to the overriding MTDs.

When the stress related to mass movements is wedded to a poorly lithified substrate (**Fa1w**), the dynamic/static overloading and rear push of the sliding mass (**Fa3n**) may, in turn, control soft-sediment deformation (*e.g.,* Butler and McCaffrey 2010; Alves and Lourenço 2010; Ogata et al. 2014). Attenuating downwards, it generally results in the development of a thick continuous deformed zone between 11% to 15% of the total thickness of the overlying MTD (Alves and Lourenço 2010; Alves 2015; Sobiesiak et al. 2018; Sobiesiak et al. 2019). Here however, the thickness of the deformation zone is almost ten times thicker than the first MTD. Notwithstanding an overestimated thickness of the deformed zone (**Fa3s**) or coalescing debris flows (**Fa3n**), one could argue that these approximations were initially calculated for a single episode of MTD emplacement, generally less than 200 meters thick (Alves and Lourenço 2010; Sobiesiak et al. 2018), and therefore do not take into consideration the cumulative effect of several episodes of mass-wasting as the ones described here. Progressive overloading of more than 400 meters (up to 900 meters) of MTDs could thus have promoted further downward propagation of the deformation front, gradually increasing its distance from the overriding MTDs. Its overall size (33% of overall MTDs) remains however highly questionable. Also, the presence of a relatively ‘undeformed' zone ~65 meters thick, which represents more than twice the size of the first MTD, here remains problematic (Figure 11; Figure 13). When an undeformed zone is sandwiched between the MTD and the deformed basal shear zone, it usually only represents a few meters of thickness, even for MTDs up to 200 meters thick (Sobiesiak et al. 2018).

Conversely, thrust propagation typically alters initial topographies and leads to the generation of a rising, laterally extensive and downward-facing slope at its front (*i.e.,* forelimb). The second episode of nappe emplacement (Glenburn Nappe) could have therefore (1) generated such a gradient leading to the downslope mass movement (*e.g.,* sliding) and deformation (*e.g.,* slumping) of the poorly lithified sediments previously deposited at its front under the action of gravity (**Fa1w** becoming **Fa3s**) (*sensu* Nardin et al. 1979), and only then, (2) triggered, through continued nappe motion and oversteepening of the forelimb gradient, the repeated failures and collapses of the front (and related pre-subduction strata), eventually resulting in the overriding mass flows (**Fa3n**) (Figure 14).

Slump-related folds are perhaps one of the most widely used indicators of the general paleoslope and transport directions (Woodcock 1979; Alsop and Marco 2011; Alsop and Weinberger 2020) and would here indicate a N-S oriented (with respect to present-day geography) paleoslope that dipped to the east (Figure 13). Such paleoslope would be consistent with being at the front (forelimb) of the seaward-moving and -verging Glenburn Nappe. Whether **Fa3s** would result, in such a scenario, from more than one slump event is difficult to ascertain. The absence of clear undeformed, horizontal horizons separating the over 300-meter-thick unit as well as the broad preferential orientation of slumping (Figure 13) rather suggests one main slide/slump event triggering a progressive soft-sediment deformation sequence (Alsop and Marco 2011). The induced continuous reworking of the early structures would, in part, explain the distribution dispersal, whereby the fold hinges gradually detach and rotate (Alsop and Marco 2011). The lateral extent of the deposits also suggests an extensive, most likely uneven slope topography, which can locally deflect the main direction of mass movement and thus, disturb the resulting slump folding patterns.

Therefore, although some substrate deformation may have locally occurred (Alves and Lourenço 2010; Alves 2015; Sobiesiak et al. 2018; Sobiesiak et al. 2019), we here interpret **Fa3s** to mainly result from mass-wasting processes that were linked to the emplacement of the Glenburn Nappe. This event not only interrupted the sustained development of the axial channel-levee system (**Fa1w**) present in the area at the time but also promoted the large-scale failure and subsequent downslope mass movements of the associated poorly lithified sedimentary cover (**Fa1w** becoming **Fa3s**) (Figure 14).

5. DISCUSSION

5.1. Insights from thrust-front mass-transport deposits

The widespread distribution (*i.e.,* along 80 kilometers of coastline and up to two kilometers wide; Figure 2; Figure 5) of the lowermost Miocene MTDs described in this study indicates that the regional tectonic settings played a significant role in triggering submarine slope failures and mass-wasting processes whereas their nature (see Section 0) and consistent location (*i.e.,* forelimb of the seaward-verging thrust sheets) suggests that they were derived from the emplacement, oversteepening and subsequent degradation of advancing thrust fronts (see also (Festa et al. 2010 and references therein) for worldwide examples and (Watson et al. 2020) for present-day examples along the Hikurangi Margin). Their extensive lateral continuity (hundreds of meters to kilometers) can be attributed to the typical sublinear morphology of the nappe front, hereby controlled by underlying thrusts.

Accepted Manuscript version. Published Journal Article version available online, published by Elsevier in Marine and Petroleum Geology Journal: https://doi.org/10.1016/j.marpetgeo.2023.106191

The different styles of MTDs and their interactions with the coeval turbidite systems however provide additional insights to the processes and controls involved (Figure 14) and can also be used to detail the overall geodynamic context in which their emplacement occurred (Figure 15).

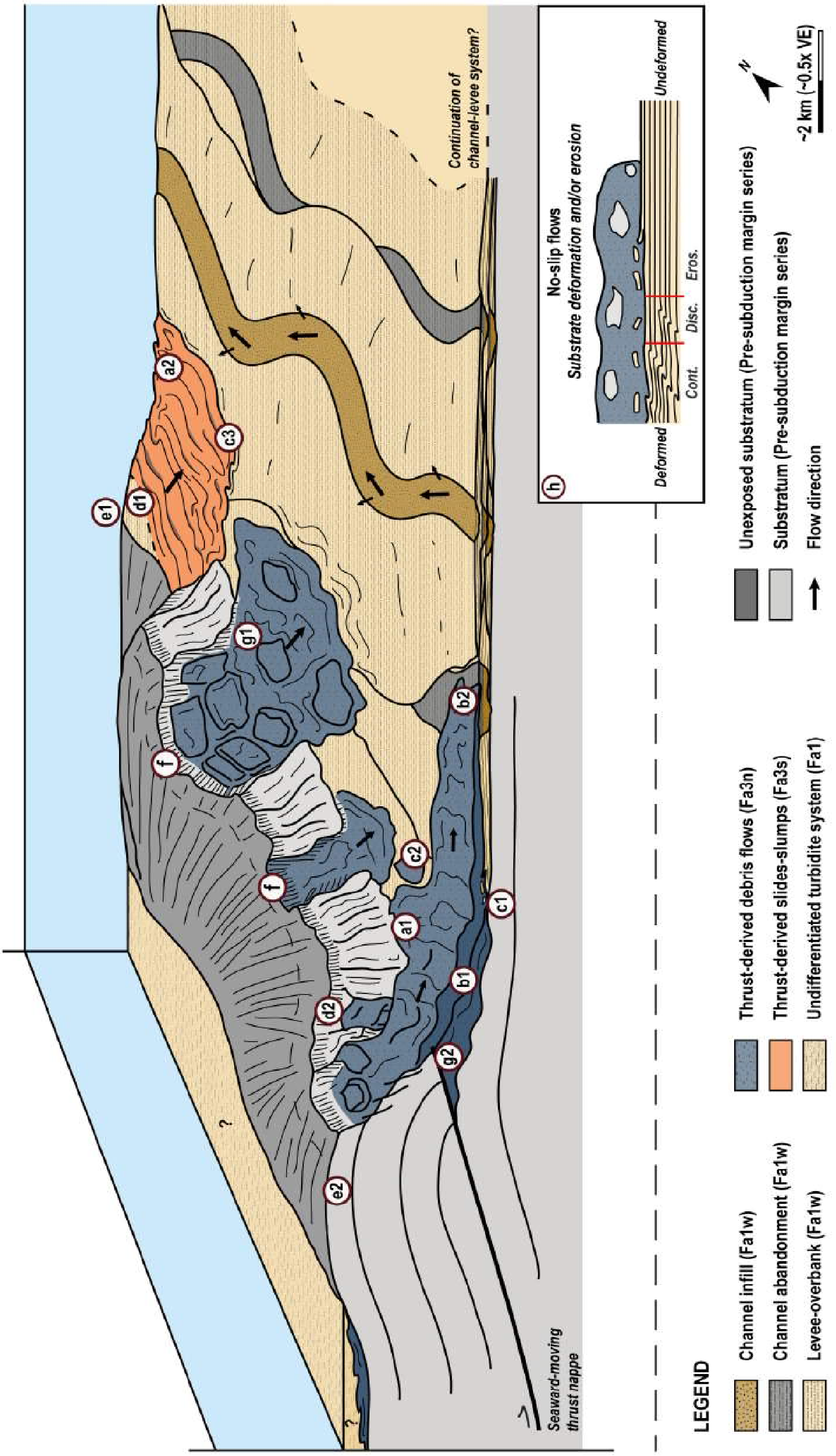

Figure 14: [previous page] Schematic representation of the processes and controls influencing the generation of mass-transport deposits at the front of thrusts in an intra-slope basin setting. (a): Styles of deposits = (a1) debrites, (a2) slides and or slumps; (b): Deposition styles = (b1) stacked, coalescing in the vicinity of the thrust, (b2) standalone, interbedded with coeval turbidite system; (c): Different interactions with the coeval turbidites = (c1) erosion, (c2) rerouting due to local irregularity of the seafloor, (c3) deformation; (d): Nature of the source = (d1) poorly-lithified sediments, (d2) lithified thrust sheet strata; (e): geometry of the source = (e1) initial rise and (e2) propagation of sublinear thrust-related fold; (f): size of the source (catchment) and its impact on the resulting deposits; (g): relation to thrust = (g1) frontal deposition, (g2) olistostromal carpet position which may be preserved from tectonic reworking due to extreme pore pressures; (h): possible styles of basal interactions from Sobiesiak et al. (2018), which could be found under the flows observed in this study. Note that there is no demonstrated relationship existing between them. Cont./Disc.: continuous or discontinuous substrate deformation. Discontinuous deformation occurs when an undeformed zone is sandwiched between the MTD and the deformed basal shear zone. Eros.: substrate erosion. VE, Vertical exaggeration.

5.1.1. Preservation at the sole of thrust sheet

Along exhumed subduction complexes, MTDs produced from sedimentary origin (*i.e.,* mass-transport processes) are commonly significantly overprinted by tectonic deformation processes and can therefore be mistaken as resulting from tectonic mechanisms (*e.g.,* offscraping, tectonic slicing) (*e.g.,* Raymond 1984; Cowan 1985; Festa et al. 2019). This long-lasting debate is particularly true for MTDs involved in thrust faulting and or found at the sole of advancing thrust sheets (*e.g.,* **Fa3n,** Table 2) (*e.g.,* Festa et al. 2016; Ogata et al. 2019).

In this study however, despite tectonic overlap, the compositional attributes of the matrix and extraformational lithoclasts (*sensu* Flores 1955; Raymond 1984) as well as the recurrent brittle-ductile syn-sedimentary deformation features (*e.g.,* Festa et al. 2016) confirmed both the sedimentary origin and mechanisms of emplacement (*i.e.,* denudation of oversteepened moving nappes) of the **Fa3n** MTDs (see Section 4.2.1; Table 2) (Chanier and Ferrière 1991). Interestingly, the Pahaoa MTDs are interpreted to be in an 'olistostromal carpet' position (*sensu* Pini et al. 2004) under the Flat Point-Whakataki Fault complex (*i.e.,* thrust) (Figure 12a) (Chanier and Ferrière 1991); yet, they do not record the traditional 'structurally ordered' and scaly-matrix fabric developing with tectonic reworking (Festa et al. 2019). Similarly, at the scale of the Flat Point outcrop, the associated MTDs and turbidites only present minor tectonic overprint even though they are located underneath the Flat Point-Whakataki Fault complex (Figure 15).

The Ocean Drilling Program (ODP) Leg 131 through the Nankai accretionary prism, offshore Japan, revealed that underthrust sediments can remain generally undeformed, possibly preserved by excess pore pressure in the *décollement* zone (Taira et al. 1992). Among others, tectonic compression and clay diagenesis (especially the smectite-illite transformation) have been widely recognized mechanisms causing extreme pore pressures (Mourgues and Cobbold 2006).

Overpressures at the sole of the Glenburn Nappe may therefore explain the preservation and relatively insignificant tectonic overprint seen in both the Pahaoa and Flat Point deposits. Instead, stress focused onto the overlying fault zone (Flat Point-Whakataki Fault complex) and resulted in several tens of meters of highly tectonized Eocene smectitic mudstones with pervasive scaly fabrics and bearing dislocated blocks of intraformational beds of glauconitic sandstones ('tectonic mélange' (*sensu* Raymond 1984; see also Pini et al. 2004; Festa et al. 2019)) (Chanier 1991; Burgreen-Chan et al. 2016; Maison et al. 2018). The scaly fabrics are strictly restricted to the thick nappe soles and do not affect the underlying overthrusted sediments, whether they are turbidites (at Flat Point) or olistostromes (at Pahaoa). As such, these examples inform that not all "olistostromal carpet" positions will result in high tectonic reworking of underlying sedimentary rocks.

5.1.2. Spatial-temporal markers of moving thrust sheets

The temporal distribution of the MTDs (**Fa3n**, **Fa3s**) and their interactions with the turbidite systems (**Fa1w**) allows a subdivision of the earliest Miocene in this part of the Hikurangi Margin into several tectonic periods (Figure 15), two of which are characterized by the coeval motion, oversteepening and frontal erosion of thrust sheets.

Through the failed material, the MTDs mostly recorded the erosion of the associated pre-subduction margin series and were used to (1) discriminate the nature of the nappe involved in a MTD, (2) specify the timing of nappe emplacement along this part of the margin and (3) better characterize the events of (submarine) exhumation and erosion.

As described by Chanier and Ferrière (1991), in the study area, the first nappe developed in the pre-subduction pelagic series, while the detrital series were still farther away to the west (Figure 4; Figure 15a). This nappe formed the landward-bounding structure of the Castlepoint trench-slope basin at the time and its dismantlement triggered both the formation of the Pahaoa MTDs, close to the thrust front and of the Flat Point and Waimimi MTDs, farther into the trench-slope basin to the east (Figure 15a).

During the same period (earliest Miocene; Figure 15c), the Castlepoint trench-slope basin was the location of a second episode of nappe emplacement, here developed in the pre-subduction intermediary to detrital series. This nappe, known as the Glenburn Nappe, was transported on the back of the seaward-verging Flat Point-Whakataki Fault complex using the Eocene smectitic mudstones as

Accepted Manuscript version. Published Journal Article version available online, published by Elsevier in Marine and Petroleum Geology Journal: https://doi.org/10.1016/j.marpetgeo.2023.106191

shallower décollement level (Figure 12a; Figure 15c) (Chanier and Ferrière 1991). The Glenburn Nappe still forms the landward bounding structure of the Castlepoint trench-slope basin today (Figure 2). Its motion led to overthrusting of the previously deposited Pahaoa and Flat Point series to the south, placing them in an 'olistostromal carpet' position (*sensu* Pini et al. 2004) and participating to the overall shortening of the area as a consequence (Figure 12a; Figure 14; Figure 15).

This rapid seaward nappe motion undoubtedly played a significant role in the dramatic emplacement of the Orui and Suicide Point MTDs, largely bigger than the Pahaoa MTDs (Appendix 5) and could, in part, be explained by the rapid development of thrust-controlled ridges during the onset of subduction. Contrary to the previous event of nappe denudation (*e.g.* Pahaoa MTDs), the analysis of the Orui and Suicide Point MTDs suggests progressive denudation of the up to 1,500 meter-thick Glenburn Nappe resulting in erosion of most (if not all) the Paleocene to Eocene strata and reaching some of its Upper Cretaceous strata (Figure 14; Figure 15c). The subsequent MTDs hold incredible thicknesses (>400 meters), considerably greater than the commonly reported thrust sheet-derived destabilization and failures (*i.e., detached* systems) (*sensu* Moscardelli and Wood 2015).

Interestingly, the emplacement of the second thrust sheet also resulted in a vertical partitioning of the mass-wasting processes at its front, to the north of the study area, as similarly observed elsewhere along the Nankai accretionary prism in Japan (*e.g.,* Strasser et al. 2011; Lackey et al. 2020).. The initial growth and steepening of the thrust forelimb promoted the failures and mass movements of the poorly lithified sediments deposited at its front (**Fa3s** at Orui), whereas the continued motion and propagation of the thrust eventually led to slope oversteepening, subsequently triggering the recurrent failures and gradual dismantlement of its forelimb (and related strata) through the emplacement of successive debris flows (**Fa3n** at Orui) (Figure 14) while also recording the progressive incorporation through time of the associated clasts in reverse stratigraphic order (Figure 11). Conversely, the nature of the substrate affected by the first thrust sheet differs to that of the second and as such, the older (*i.e.,* non-coeval) semi-lithified pre-subduction strata might instead explain the absence of vertical partitioning at the front of the first thrust sheet (Figure 12a). At Pahaoa, the mass-flow deposits (**Fa3n**) directly overlie the (undeformed) pre-subduction strata, depositing above a geological contact with pyrite concretions (hard ground), witness of an Oligocene sedimentary hiatus in this area (Chanier and Ferrière 1991; Morgans and Hollis 2000).

Overall, the variations encountered in the nature and size of the MTDs indicate that (1) the outboard migration of deformation was uneven during the earliest Miocene and punctuated by the emplacement and motions of two distinct thrust sheets, displaying longitudinal and lateral variations along the margin,

Accepted Manuscript version. Published Journal Article version available online, published by Elsevier in Marine and Petroleum Geology Journal: https://doi.org/10.1016/j.marpetgeo.2023.106191

and that (2) the frontal denudation of a nappe generally resulted from a series of destabilizations, rather than only one event, and thus promoted the gradual (submarine) exhumation and erosion of its substratum.

Notwithstanding the nature and topography of the overridden substratum as another contributor (*e.g.,* Ortiz-Karpf et al. 2017), the source areas here appear to have chiefly controlled the lateral and vertical variations encountered in both the morphometric parameters (*e.g.,* lateral extent, overall thickness) and nature of lithoclasts of the MTDs (**Fa3n,** Table 2). The thrust sheet involved not only generated a specific type of failed material related to the nature of its substrate, but also provided different catchment sizes from the nappe thickness (Pahaoa vs Orui MTDs) (Figure 14). Contrasting magnitude of mass-wasting events linked to both regional and local tectonics (*e.g.,* variation in thrust angle, convergent deformation rate, seismicity) can also be considered to explain the locally varying recurrence, erosive magnitude and size of the resulting MTDs.

5.2. Early stages of trench-slope basin development

At their early stages of development, trench-slope basins are typically narrow (five to 10 kilometers wide) (Bailleul et al. 2013). Often located downslope (*i.e.,* towards the base of the lower trench-slope) at that time, they are supposed to be sedimentologically 'immature' (*sensu* Underwood and Bachman 1982), being disconnected from the main sediment pathways that cross the margin. The tectonostratigraphic development of the Castlepoint trench-slope basin, contemporaneous with the beginning of the subduction, deviates from this model.

As previously suggested by Turnbull (1988), Field (2005) and Sloss et al. (2021), the consistent axial routing of the turbidite paleoflows within the channel-levee system (**Fa1w,** Table 2) outlines the presence of a sublinear bathymetry to the east, which was likely controlled by an underlying thrust. This bathymetry formed an outboard basin-bounding structure at the time (earliest Miocene), and thus provided an elongate shape to the Castlepoint trench-slope basin. The basin likely formed a wide structural depression in its early stages recording the coeval development of gravity-driven systems at least ~12 to 15 kilometers apart (minimum orthogonal distance between Pahaoa and Flat Point deposits nowadays) (Figure 15). The emplacement of the inboard second thrust sheet (*i.e.,* Glenburn Nappe) produced a shortening with overthrusting of its western part (Figure 15). Such structural control is intrinsically linked to the initial stages of development of the Hikurangi Margin (Chanier and Ferrière 1989; Chanier and Ferrière 1991; Rait et al. 1991; Nicol et al. 2007; Bailleul et al. 2013; Bland et al. 2022), characterized by initial deformation of the previous margin and seaward nappe emplacement. It therefore informs that several thrusts can control the development of the tectonically active, sublinear bathymetric highs that delineate a trench-slope basin, as also observed elsewhere from offshore seismic reflection data (*e.g.,* Nankai: (Gulick et al. 2004) and Hikurangi Margins: (Barnes et al. 2010; Bland et al. 2015; McArthur et al. 2019; Griffin et al. 2022)).

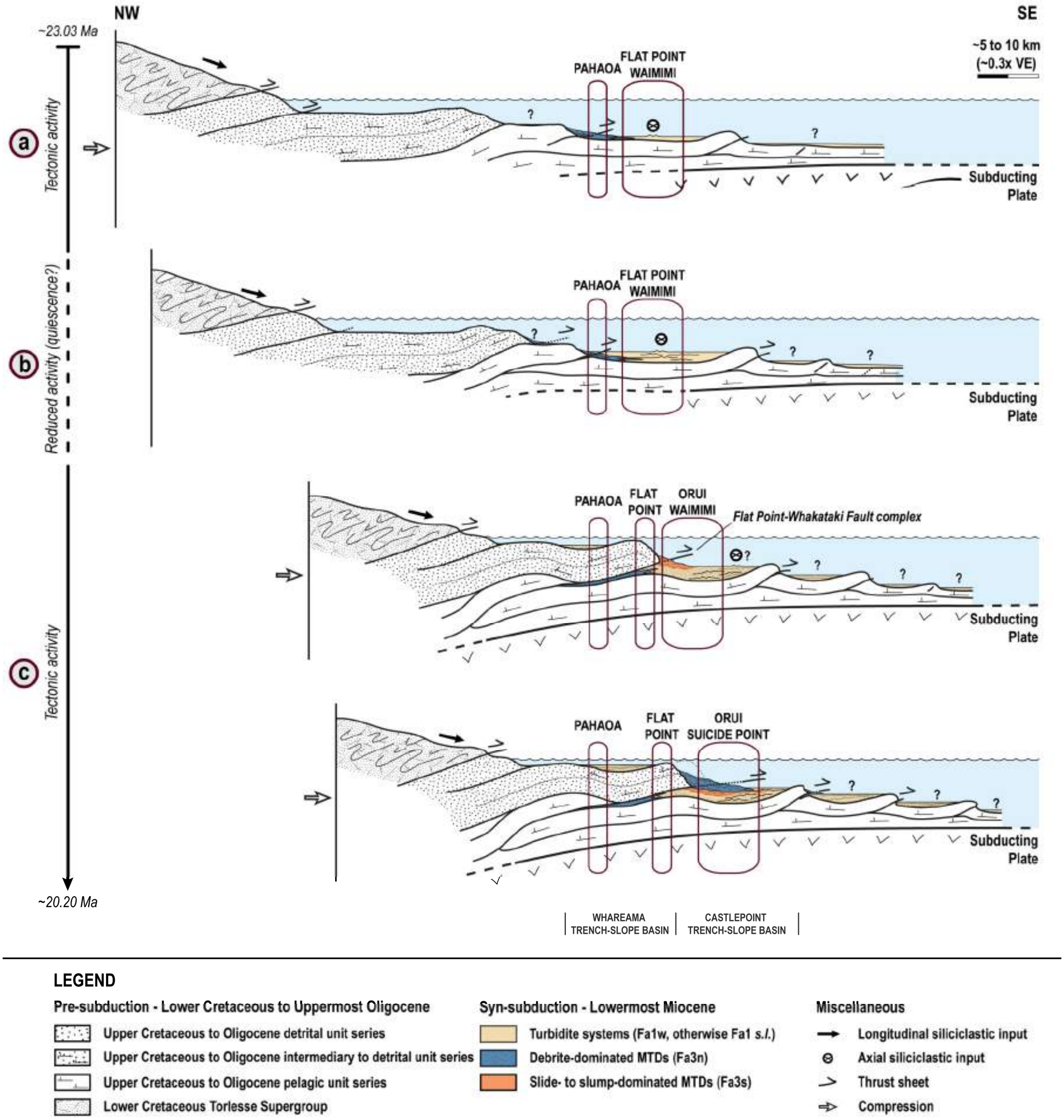

Figure 15: Schematic NW-SE cross-sections reconstructing the tectonostratigraphic development of the southern Hikurangi subduction wedge during the Early Miocene. These cross-sections specifically focus on the Castlepoint trench-slope basin, and highlight the evolution in depositional settings through time, encountered at the Pahaoa, Flat Point, Orui, Waimimi and Suicide Point localities described in the text. VE, Vertical exaggeration. Inspired from Chanier (1991).

Accepted Manuscript version. Published Journal Article version available online, published by Elsevier in Marine and Petroleum Geology Journal: https://doi.org/10.1016/j.marpetgeo.2023.106191

Contemporaneously, mixed gravity-driven sedimentation prevailed during the early fill of the Castlepoint trench-slope basin, featuring both the emplacement of (1) locally-derived MTDs (**Fa3s**, **Fa3n**) and (2) hinterland-derived turbidite systems (**Fa1w**) (Table 2; Figure 15). These two contrasting sources of sediment supply are not only local and from bathyal water depths, but also connected to a perennial nearshore system, and thus indicate that the trench-slope basin was sedimentologically 'mature' (*sensu* Underwood and Bachman 1982) as soon as its initial fill started.

This contrasts with the interpretation of Sloss et al. (2021) inferring that the Castlepoint trench-slope basin was 'immature' (*sensu* Underwood and Bachman 1982) and instead suggests that the basin floor of the Castlepoint trench-slope basin was reached by submarine canyons, maintaining their channels downslope, very early in the history of the convergent Hikurangi margin. Such phenomena may have been favored by a young, narrow subduction wedge, where the distance down the lower trench-slope was reduced and with it, the number of active thrust ridges. This would have, in turn, increased the chances for canyon and or slope channel systems to connect and remain connected with the trench-slope basins downslope. The coeval episodes of submarine destabilization and collapses, essentially recorded at the front (*i.e.,* forelimb) of the landward basin-bounding structure however indicates that the associated thrust ridge(s) remained active, probably still in close proximity with the deformation front.

Interestingly, the associated turbidite deposits (**Fa1w**) do not appear strongly influenced by syn-depositional tectonics, recording the development of a several hundreds of meters thick aggradational channel-levee system along the Castlepoint trench-slope basin (>50 kilometers long) (Figure 8; Figure 9; Figure 14; Figure 15a, b). This depositional architecture not only contrasts with previous interpretations inferred for the area now occupied by the southern coastal ranges (Chanier and Ferrière 1991; Neef 1992; Bailleul et al. 2007; Sloss et al. 2021) and lower trench-slope basins in general (Underwood and Bachman 1982; Underwood and Moore 1995), but also suggests that (1) the destructive compressional deformation affecting the margin at the time was uneven along the margin and or that (2) a balance between the controlling parameters (*e.g.,* sea-level changes, tectonics, sediment fluxes) was locally maintained as demonstrated elsewhere by McArthur et al. (2021) (lobe deposits of the onshore Akitio and offshore Porangahau trench-slope basins, Hikurangi Margin).

Much work has been done on basin floor aggradational channel-levee complexes (*e.g.,* Kolla et al. 2007; Armitage et al. 2012; Jobe et al. 2020); and notwithstanding their impact on the sediment supply or hinterland conditions, sea-level changes are often considered to have limited effects on the vertical organization of deep-marine channels (Kolla et al. 2007). Conversely, the feedback mechanism coupling structure growth and sediment loading proposed by McArthur et al. (2021) can explain the prolonged

Accepted Manuscript version. Published Journal Article version available online, published by Elsevier in Marine and Petroleum Geology Journal: https://doi.org/10.1016/j.marpetgeo.2023.106191

generation of accommodation in a trench-slope basin and allow continued sediment deposition forming large-scale aggradational systems.

Such a model implies a balanced interaction between load-driven subsidence in the basin and tectonic activity focused at the bounding structures, whilst providing a relatively stable depocenter within the basin. This focused tectonic activity (*e.g.,* vertical and or horizontal motion) chiefly controlled the sediment distribution and architecture in the trench-slope basin (*e.g.,* Vinnels et al. 2010), alternatively maintaining direct input from the upper slope settings and or promoting remobilization from the downslope bathymetric highs (Figure 15a, b). Such feedback mechanism therefore suggests that even during the early stages of structural development of a subduction margin, some 'mature' trench-slope basin fills can reach a balance between active tectonics and sedimentation.

External forcing factors, such as the second event of moving thrust sheets (*i.e.,* Glenburn Nappe), eventually disrupted the sedimentation-deformation equilibrium and drastically transformed the sedimentation style recorded within the Castlepoint trench-slope basin *(e.g.,* from a long-lasting channel-levee system (**Fa1w**) to large-scale MTDs (**Fa3n**)) (Figure 15c).

Accepted Manuscript version. Published Journal Article version available online, published by Elsevier in Marine and Petroleum Geology Journal: https://doi.org/10.1016/j.marpetgeo.2023.106191

6. CONCLUSIONS

New observations are drawn from this outcrop-based study on the initial development of the Hikurangi subduction wedge (eastern North Island of New Zealand). The high-resolution analysis of the different styles of mass-transport deposits (MTDs) and their interactions with a coeval turbidite system permits fresh insights on the structural evolution and stratigraphic infill of one of the oldest trench-slope basins (the Castlepoint trench-slope basin) of the Hikurangi subduction zone.

MTDs are powerful spatial-temporal markers of geologic events. They have allowed us to discriminate the nature of the nappes responsible for shedding each MTD, to specify the timing of nappe emplacement along this part of the margin, and to provide significant clues for understanding the tectonostratigraphic evolution of both the intra-slope basin and the Hikurangi Margin.

(1) The matrix-supported pebbly conglomerates described in this study were produced from sedimentary processes (*i.e.,* MTDs). Although some were found at the sole of the thrust sheets, they were not always significantly overprinted by tectonic deformation processes (*i.e.,* tectonic mélanges). Tectonic reworking of underthrust deposits (*e.g.,* MTDs) should therefore not always be expected from olistostromal carpet positions, since overpressures at the sole of the overlying thrust sheet may instead favor their preservation and only result in minor tectonic deformation.

(2) Oversteepened slopes at the front of advancing thrust sheets were the main causal mechanism for the mass-wasting processes described here and resulted in a series of (rather than one) destabilization events, dominated by mass flows. The thrust sheet involved not only generated a specific type of failed material related to the nature of its substrate but also provided different catchment (and resulting deposit) sizes from the nappe thickness. When affecting poorly lithified sediments however, the thrust faults were seen to control the generation of different styles of MTDs at their front, showing a vertical partitioning of the mass-wasting processes, (1) first dominated by mass movements (*e.g.,* sliding, slumping) and (2) then by mass flows (*e.g.,* debris flows). The initial growth and steepening of the thrust forelimb flank promoted the failures and mass movements of the poorly lithified sediments deposited at its front, whereas continued thrust propagation eventually led to oversteepening, subsequently triggering the recurrent failures and gradual dismantlement of its forelimb (and associated core strata) through the emplacement of successive mass flows.

(3) The associated deposits are essentially captured in close vicinity to the thrust sheet front where they form a series of stacked MTDs. Commonly referred to as *detached* systems, they here characteristically comprise less than three square kilometers in area and a few kilometers in width and length. The Orui and Suicide Point MTDs however show remarkable thicknesses (greater than 400 meters). Interestingly, the mass flow deposits record the denudation of their source (*i.e.,* thrust sheets) with progressive incorporation through time of clasts in reverse stratigraphic order.

(4) Surprisingly for trench-slope basins coeval with the birth of a subduction margin, the early stages of their fill development can deviate from the classical models either showing (1) a direct connection of the basin with sustainable sediment sources making them 'mature' (*sensu* Underwood and Bachman 1982) very early in the history of the convergent margin, and (2) the occurrence of sedimentation-deformation feedback mechanism(s) resulting in the development of a several hundreds of meters thick aggradational turbidite system sourced from shallow waters and maintained downslope.

(5) The outboard migration of deformation during the Early Miocene period of compressional deformation was discontinuous and uneven along the Hikurangi Margin. In the study area, two major tectonic events were recorded at one of the trench-slope basin edges, separated by a period of reduced tectonic activity. Each tectonic event or pulse lasted approximatively of 1 to 2 Myrs in duration and resulted in seaward motion, oversteepening and frontal denudation of a thrust sheet. The second nappe overthrusted the preceding, thereby forming a succession of two superposed nappes and participating to the overall shortening of the area. As a result, not only one but several stacked seaward-verging thrust sheets were observed to control the tectonically active sublinear bathymetric high that delineated the landward margin of the Castlepoint trench-slope basin at the time.

(6) Finally, important thrust ridges existed since the earliest Miocene, late Waitakian-Otaian. One of them, controlled by the underlying Flat Point-Whakataki Fault complex, formed and still forms the basin-bounding structure separating the 'Whareama trench-slope basin' (since the earliest Miocene, late Waitakian-Otaian) and the 'Akitio trench-slope basin' (since at least the Middle Miocene, Altonian) from the 'Castlepoint trench-slope basin', a newly identified sub-basin to the East Coast Basin domain, which started to develop contemporaneously with the onset of subduction.

Accepted Manuscript version. Published Journal Article version available online, published by Elsevier in Marine and Petroleum Geology Journal: https://doi.org/10.1016/j.marpetgeo.2023.106191

7. AKNOWLEDGEMENTS

This research was funded by Schlumberger. We genuinely thank Karen and John Barbour for their heartfelt welcome during our stays at Homewood and for easing our access to the studied areas. Special thanks to Corentin Chaptal, Andréa Barrier, Mylène Receveur and Vincent Caron for their incredible support during the fieldwork missions. We also thank the BSc students who helped creating the 3D outcrop models. We are forever grateful to Hugh Morgans from GNS Science (Lower Hutt, New Zealand) for his paleontological analyses and to our colleagues from the Basins-Reservoirs-Resources B2R research unit (University of UniLaSalle, France) for their lasting support. Finally, we thank the Editor Kai Ogata and the reviewers, Kyle Bland and an anonymous reviewer, for their helpful and constructive comments and suggestions.

8. REFERENCES

Alsop GI, Marco S. 2011. Soft-sediment deformation within seismogenic slumps of the Dead Sea Basin. Journal of Structural Geology. 33(4):433–457. https://doi.org/10.1016/j.jsg.2011.02.003

Alsop GI, Weinberger R. 2020. Are slump folds reliable indicators of downslope flow in recent mass transport deposits? Journal of Structural Geology. 135:104037. https://doi.org/10.1016/j.jsg.2020.104037

Alves TM. 2015. Submarine slide blocks and associated soft-sediment deformation in deep-water basins: A review. Marine and Petroleum Geology. 67:262–285. https://doi.org/10.1016/j.marpetgeo.2015.05.010

Alves TM, Lourenço SDN. 2010. Geomorphologic features related to gravitational collapse: Submarine landsliding to lateral spreading on a Late Miocene–Quaternary slope (SE Crete, eastern Mediterranean). Geomorphology. 123(1):13–33. https://doi.org/10.1016/j.geomorph.2010.04.030

Armitage DA, McHargue T, Fildani A, Graham SA. 2012. Postavulsion channel evolution: Niger Delta continental slopeNigeria Avulsions. AAPG Bulletin. 96(5):823–843. https://doi.org/10.1306/09131110189

Armitage DA, Romans BW, Covault JA, Graham SA. 2009. The Influence of Mass-Transport-Deposit Surface Topography on the Evolution of Turbidite Architecture: The Sierra Contreras, Tres Pasos Formation (Cretaceous), Southern Chile. Journal of Sedimentary Research. 79(5):287–301. https://doi.org/10.2110/jsr.2009.035

Bailleul J, Chanier F, Ferrière J, Robin C, Nicol A, Mahieux G, Gorini C, Caron V. 2013. Neogene evolution of lower trench-slope basins and wedge development in the central Hikurangi subduction margin, New Zealand. Tectonophysics. 591:152–174. https://doi.org/10.1016/j.tecto.2013.01.003

Bailleul J, Robin C, Chanier F, Guillocheau F, Field B, Ferrière J. 2007. Turbidite Systems in the Inner Forearc Domain of the Hikurangi Convergent Margin (New Zealand): New Constraints on the Development of Trench-Slope Basins. Journal of Sedimentary Research. 77(4):263–283. https://doi.org/10.2110/jsr.2007.028

Ballance PF. 1976. Evolution of the Upper Cenozoic Magmatic Arc and plate boundary in northern New Zealand. Earth and Planetary Science Letters. 28(3):356–370. https://doi.org/10.1016/0012-821X(76)90197-7

Barnes PM, Korsch RJ. 1990. Structural analysis of a middle Cretaceous accretionary wedge, Wairarapa, New Zealand. New Zealand Journal of Geology and Geophysics. 33(2):355–375. https://doi.org/10.1080/00288306.1990.10425693

Barnes PM, Korsch RJ. 1991. Melange and related structures in Torlesse accretionary wedge, Wairarapa, New Zealand. New Zealand Journal of Geology and Geophysics. 34(4):517–532. https://doi.org/10.1080/00288306.1991.9514487

Barnes PM, Lamarche G, Bialas J, Henrys S, Pecher I, Netzeband GL, Greinert J, Mountjoy JJ, Pedley K, Crutchley G. 2010. Tectonic and geological framework for gas hydrates and cold seeps on the Hikurangi subduction margin, New Zealand. Marine Geology. 272(1–4):26–48. https://doi.org/10.1016/j.margeo.2009.03.012

Beavan J, Tregoning P, Bevis M, Kato T, Meertens C. 2002. Motion and rigidity of the Pacific Plate and implications for plate boundary deformation. Journal of Geophysical Research: Solid Earth. 107(B10):ETG 19-1-ETG 19-15. https://doi.org/10.1029/2001JB000282

Biros D, Cuevas R, Moehl B. 1995. Well completion report, Titihaoa-1. PPL 38318. New Zealand.

Bland KJ, Morgans HEG, Strogen DP, Harvey H. 2022. Litho- and biostratigraphy of a late Oligocene–Early Miocene succession in the Weber area, southern Hawke's Bay, and implications for early Hikurangi subduction-margin evolution. New Zealand Journal of Geology and Geophysics.:1–24. https://doi.org/10.1080/00288306.2022.2108069

Bland KJ, Uruski CI, Isaac MJ. 2015. Pegasus Basin, eastern New Zealand: A stratigraphic record of subsidence and subduction, ancient and modern. New Zealand Journal of Geology and Geophysics. 58(4):319–343. https://doi.org/10.1080/00288306.2015.1076862

Bouma AH. 1962. Sedimentology of some Flysch deposits: a graphic approach to facies interpretation [PhD Thesis]. Amsterdam, Netherlands: Elsevier.

Bradshaw JD. 1989. Cretaceous geotectonic patterns in the New Zealand Region. Tectonics. 8(4):803–820. https://doi.org/10.1029/TC008i004p00803

Bull S, Cartwright J, Huuse M. 2009. A review of kinematic indicators from mass-transport complexes using 3D seismic data. Marine and Petroleum Geology. 26:1132–1151.

Burgreen-Chan B, Meisling KE, Graham S. 2016. Basin and petroleum system modelling of the East Coast Basin, New Zealand: a test of overpressure scenarios in a convergent margin. Basin Research. 28(4):536–567. https://doi.org/10.1111/bre.12121

Butler RWH, McCaffrey WD. 2010. Structural evolution and sediment entrainment in mass-transport complexes: outcrop studies from Italy. Journal of the Geological Society. 167(3):617–631. https://doi.org/10.1144/0016-76492009-041

Chanier F. 1991. Le prisme d'accrétion Hikurangi: un témoin de l'évolution géodynamique d'une marge active pacifique (Nouvelle-Zélande) [PhD Thesis]. France: Université de Lille 1.

Chanier F, Bellier J-P, Bignot G, Ferrière J. 1990. Discovery of Pithonellids in the Upper Cretaceous of New Zealand; biogeographic, stratigraphic and tectonic consequences. Comptes Rendus de l'Académie des Sciences - Séries II - Earth and Planetary Science. 310(2):1095–1100.

Chanier F, Ferrière J. 1989. On the existence of major tangential movements in the East Coast Range of New Zealand: their significance within the framework of Pacific plate subduction. Comptes Rendus de l'Académie des Sciences - Séries II - Earth and Planetary Science. 308(2):1645–1650.

Chanier F, Ferrière J. 1991. From a passive to an active margin: Tectonic and sedimentary processes linked to the birth of an accretionary prism (Hikurangi Margin, New Zealand). Société Géologique de France. 162(4):649–660. https://doi.org/10.2113/gssgfbull.162.4.649

Chanier F, Ferrière J, Angelier J. 1999. Extensional deformation across an active margin, relations with subsidence, uplift, and rotations: The Hikurangi subduction, New Zealand. Tectonics. 18(5):862–876. https://doi.org/10.1029/1999TC900028

Claussmann B, Bailleul J, Chanier F, Caron V, McArthur AD, Mahieux G, Chaptal C, Vendeville BC. 2021. Contrasting mixed siliciclastic-carbonate shelf-derived gravity-driven systems in compressive intra-slope basins (southern Hikurangi margin, New Zealand). Marine and Petroleum Geology. http://dx.doi.org/10.1016/j.marpetgeo.2021.105252

Claussmann B, Bailleul J, Chanier F, Mahieux G, Caron V, McArthur AD, Chaptal C, Morgans HEG, Vendeville BC. 2022. Shelf-derived mass-transport deposits: origin and significance in the stratigraphic development of trench-slope basins. New Zealand Journal of Geology and Geophysics. 1:1–36. https://doi.org/10.1080/00288306.2021.1918729

Clowes CD, Crampton JS, Bland KJ, Collins KS, Prebble JG, Raine JI, Strogen DP, Terezow MG, Womack T. 2021. The New Zealand Fossil Record File: a unique database of biological history. New Zealand Journal of Geology and Geophysics. 64(1):62–71. https://doi.org/10.1080/00288306.2020.1799827

Cooper RA, editor. 2004. The New Zealand Geological Timescale. Lower Hutt, New Zealand: Institute of Geological & Nuclear Sciences Limited.

Cowan DS. 1985. Structural styles in Mesozoic and Cenozoic mélanges in the western Cordillera of North America. GSA Bulletin. 96(4):451–462. https://doi.org/10.1130/0016-7606(1985)96<451:SSIMAC>2.0.CO;2

Crampton JS. 1997. The Cretaceous stratigraphy of the southern Hawke's Bay-Wairarapa region. Lower Hutt, New Zealand: Institute of Geological & Nuclear Sciences.

Crampton JS, Mortimer N, Bland KJ, Strogen DP, Sagar M, Hines BR, King PR, Seebeck H. 2019. Cretaceous termination of subduction at the Zealandia margin of Gondwana: The view from the paleo-trench. Gondwana Research. 70:222–242. https://doi.org/10.1016/j.gr.2019.01.010

Crundwell M, Scott GH, Thrasher GP. 1994. Calibration of paleobathymetry indicators by integrated seismic and paleontological analysis of forest sequences, Taranaki Basin, New Zealand. In: Proceedings of the New Zealand Petroleum Conference. Wellington, New Zealand; p. 169–178.

Delteil J, Lepinay BM de, Morgans HEG, Field BD. 2006. Olistostromes marking tectonic events, East Coast, New Zealand. New Zealand Journal of Geology and Geophysics. 49(4):517–531. https://doi.org/10.1080/00288306.2006.9515185

Delteil J, Morgans HEG, Raine JI, Field BD, Cutten HNC. 1996. Early Miocene thin-skinned tectonics and wrench faulting in the Pongaroa district, Hikurangi margin, North Island, New Zealand. New Zealand Journal of Geology and Geophysics. 39(2):271–282. https://doi.org/10.1080/00288306.1996.9514711

Down TN. 2016. Structural-stratigraphic reconstruction of the Lower Whakataki Formation, North Island, New Zealand [MSc Thesis]. Australia: Faculty of Science and Engineering Queensland University of Technology.

Edbrooke SW, Browne GH. 1996. An Outcrop Study of Bed Thickness and Continuity in Thin-bedded Facies of the Whakataki Formation at Whakataki Beach, East Wairarapa. New Zealand: Institute of Geological & Nuclear Sciences.

Festa A, Ogata K, Pini GA, Dilek Y, Alonso JL. 2016. Origin and significance of olistostromes in the evolution of orogenic belts: A global synthesis. Gondwana Research. 39:180–203. https://doi.org/10.1016/j.gr.2016.08.002

Festa A, Pini GA, Dilek Y, Codegone G. 2010. Mélanges and mélange-forming processes: a historical overview and new concepts. International Geology Review. 52(10–12):1040–1105. https://doi.org/10.1080/00206810903557704

Festa A, Pini GA, Ogata K, Dilek Y. 2019. Diagnostic features and field-criteria in recognition of tectonic, sedimentary and diapiric mélanges in orogenic belts and exhumed subduction-accretion complexes. Gondwana Research. 74:7–30. https://doi.org/10.1016/j.gr.2019.01.003

Field BD. 2005. Cyclicity in turbidites of the Miocene Whakataki Formation, Castlepoint, North Island, and implications for hydrocarbon reservoir modelling. New Zealand Journal of Geology and Geophysics. 48(1):135–146. https://doi.org/10.1080/00288306.2005.9515104

Field BD, Uruski CI, Beu AG, Browne GH, Crampton JS, Funnel RH, Killops SD, Laird M, Mazengarb C, Morgans HEG, Others. 1997. Cretaceous-Cenozoic geology and petroleum systems of the East Coast region, New Zealand. New Zealand.

Fisher RV. 1983. Flow transformations in sediment gravity flows. Geology. 11(5):273–274.

Flores G. 1955. Les résultats des études pour les recherches pétroliféres en Sicile: discussion. In: Proceedings of the 4th world petroleum congress. Rome, Italia.

Folk RL. 1954. The Distinction between Grain Size and Mineral Composition in Sedimentary-Rock Nomenclature. The Journal of Geology. 62(4):344–359.

Galloway WE. 1998. Siliciclastic Slope and Base-of-Slope Depositional Systems: Component Facies, Stratigraphic Architecture, and Classification. AAPG Bulletin. 824:569–595. https://doi.org/10.1306/1D9BC5BB-172D-11D7-8645000102C1865D

George AD. 1990. Deformation processes in an accretionary prism: a study from the Torlesse terrane of New Zealand. Journal of Structural Geology. 12(5):747–759. https://doi.org/10.1016/0191-8141(90)90086-E

George AD. 1992. Deposition and deformation of an Early Cretaceous trench-slope basin deposit, Torlesse terrane, New Zealand. GSA Bulletin. 104(5):570–580. https://doi.org/10.1130/0016-7606(1992)104<0570:DADOAE>2.3.CO;2

Ghisetti F, Barnes P, Ellis S, Plaza A, Barker D. 2016. The last 2 Myr of accretionary wedge construction in the central Hikurangi margin (North Island, New Zealand): Insights from structural modeling. Geochemistry, Geophysics, Geosystems. 17:1–26. https://doi.org/10.1002/2016GC006341

Griffin AG, Bland KJ, Morgans HEG, Strogen DP. 2022. A multifaceted study of the offshore Titihaoa-1 drillhole and a Neogene accretionary slope basin, Hikurangi subduction margin. New Zealand Journal of Geology and Geophysics. 65(1):79–104. https://doi.org/10.1080/00288306.2021.1932527

Gulick SPS, Bangs NLB, Shipley TH, Nakamura Y, Moore GF, Kuramoto S. 2004. Three-dimensional architecture of the Nankai accretionary prism's imbricate thrust zone off Cape Muroto, Japan: Prism reconstruction via en echelon thrust propagation. Journal of Geophysical Research: Solid Earth. 109(B2). https://doi.org/10.1029/2003JB002654

Hayward BW, Black PM, Smith IEM, Ballance PF, Itaya T, Doi M, Takagi M, Bergman S, Adams CJ, Herzer RH, Robertson DJ. 2001. K-Ar ages of early Miocene arc-type volcanoes in northern New Zealand. New Zealand Journal of Geology and Geophysics. 44(2):285–311. https://doi.org/10.1080/00288306.2001.9514939

Hayward BW (Bruce W, New Zealand Geological Survey Paleontology Group. 1986. A guide to paleoenvironmental assessment using New Zealand Cenozoic forminiferal :i.e. foraminiferal: faunas. Lower Hutt, New Zealand: New Zealand Geological Survey.

Hayward BW, Kawagata S, Sabaa A, Grenfell H, van Kerchhoven L, Johnson K, Thomas E. 2012. The last global extinction (Mid-Pleistocene) of deep-sea benthic Foraminifera (Chrysalogoniidae, Ellipsoidinidae, Glandulonodosariidae, Plectofrondiculariidae, Pleurostomellidae, Stilostomellidae): their late Cretaceous-Cenozoic history and taxonomy. Fredericksburg, USA: Cushman Foundation for Foraminiferal Research.

Hines B. 2018. Cretaceous to Paleogene Palinspastic Reconstruction of the East Coast Basin, New Zealand [PhD Thesis] [Internet]. Wellington, New Zealand: Victoria University; [accessed 2023 Jan 13]. http://researcharchive.vuw.ac.nz/handle/10063/7715

Hines B, Kulhanek D, Hollis C, Atkins C, Morgans H. 2013. Paleocene–Eocene stratigraphy and paleoenvironment at Tora, Southeast Wairarapa, New Zealand. New Zealand Journal of Geology and Geophysics. 56(4):243–262. https://doi.org/10.1080/00288306.2013.836112

Hines BR, Seebeck H, Crampton JS, Bland KJ, Strogen DP. 2022. Reconstructing a dismembered Neogene basin along the active Hikurangi subduction margin, New Zealand. GSA Bulletin [Internet]. [accessed 2023 Jan 13]. https://doi.org/10.1130/B36308.1

Hodgson DM, Kane IA, Flint SS, Brunt RL, Ortiz-Karpf A. 2016. Time-transgressive Confinement On the Slope and the Progradation of Basin-floor Fans: Implications For the Sequence Stratigraphy of Deep-water Deposits. Journal of Sedimentary Research. 86(1):73–86. https://doi.org/10.2110/jsr.2016.3

Hollis CJ, Tayler MJS, Andrew B, Taylor KW, Lurcock P, Bijl PK, Kulhanek DK, Crouch EM, Nelson CS, Pancost RD, et al. 2014. Organic-rich sedimentation in the South Pacific Ocean associated with Late Paleocene climatic cooling. Earth-Science Reviews. 134:81–97. https://doi.org/10.1016/j.earscirev.2014.03.006

Hornibrook N de B, Strong CP, Brazier RC. 1989. Manual of New Zealand Permian to Pleistocene foraminiferal biostratigraphy. Lower Hutt, New Zealand: New Zealand Geological Survey.

Iverson RM. 1997. The physics of debris flows. Reviews of Geophysics. 35(3):245–296. https://doi.org/10.1029/97RG00426

Jenkins DG. 1971. New Zealand Cenozoic Planktonic Foraminifera. Lower Hutt, New Zealand: New Zealand Geological Survey.

Jobe ZR, Howes NC, Straub KM, Cai D, Deng H, Laugier FJ, Pettinga LA, Shumaker LE. 2020. Comparing Aggradation, Superelevation, and Avulsion Frequency of Submarine and Fluvial Channels. Frontiers in Earth Science. 8. https://doi.org/10.3389/feart.2020.00053

Johnston MR. 1980. Geology of the Tinui-Awatoitoi district. Wellington, New Zealand: New Zealand Dept of Scientific and Industrial Research.

Jones OT. 1944. The compaction of muddy sediments. Quarterly Journal of the Geological Society. 100(1–4):137–160. https://doi.org/10.1144/GSL.JGS.1944.100.01-04.09

Kane IA, Hodgson DM. 2011. Sedimentological criteria to differentiate submarine channel levee subenvironments: Exhumed examples from the Rosario Fm. (Upper Cretaceous) of Baja California, Mexico, and the Fort Brown Fm. (Permian), Karoo Basin, S. Africa. Marine and Petroleum Geology. 28(3):807–823. https://doi.org/10.1016/j.marpetgeo.2010.05.009

Karig DE, Moore GF, Curray JR, Lawrence MB. 1980. Morphology and shallow structure of the lower trench slope off Nias Island, Sunda Arc. In: Hayes DE, editor. The Tectonic and Geologic Evolution of Southeast Asian Seas and Islands. Washington, America; p. 179–208.

Karig DE, Sharman GF. 1975. Subduction and Accretion in Trenches. GSA Bulletin. 86(3):377–389. https://doi.org/10.1130/0016-7606(1975)86<377:SAAIT>2.0.CO;2

King PR. 2000. Tectonic reconstructions of New Zealand: 40 Ma to the Present. New Zealand Journal of Geology and Geophysics. 43(4):611–638. https://doi.org/10.1080/00288306.2000.9514913

Kolla V, Posamentier HW, Wood LJ. 2007. Deep-water and fluvial sinuous channels—Characteristics, similarities and dissimilarities, and modes of formation. Marine and Petroleum Geology. 24(6):388–405. https://doi.org/10.1016/j.marpetgeo.2007.01.007

Kuenen PhH. 1964. Deep-Sea Sands and Ancient Turbidites. In: Bouma AH, Brouwer A, editors. Developments in Sedimentology. Vol. 3. Netherlands: Elsevier; p. 3–33. https://doi.org/10.1016/S0070-4571(08)70953-1

Lackey JK, Regalla CA, Moore GF. 2020. Tectonic Influences on Trench Slope Basin Development via Structural Restoration Along the Outer Nankai Accretionary Prism, Southwest Japan. Geochemistry, Geophysics, Geosystems. 21(8):1–17.

Lee J, Begg J. 2002. Geology of the Wairarapa area. Institute of Geological & Nuclear Sciences 1:250 000 geological map: Institute of Geological & Nuclear Sciences Limited.

Lewis KB, Barnes PM, Garlick RD. 1999. Central Hikurangi GeodyNZ swath maps: depths, texture and geological interpretation.

Lewis KB, Pettinga JR. 1993. The emerging, imbricate frontal wedge of the Hikurangi margin. In: Ballance PF, editor. South Pacific sedimentary basins. Amsterdam, Netherlands: Elsevier Science; p. 225–250.

van der Lingen GJ. 1982. Development of the North Island Subduction System, New Zealand. Geological Society, London, Special Publications. 10(1):259–272. https://doi.org/10.1144/GSL.SP.1982.010.01.17

van der Lingen GJ, Pettinga JR. 1980. The Makara Basin: A Miocene Slope-Basin along the New Zealand Sector of the Australian-Pacific Obliquely Convergent Plate Boundary. In: Sedimentation in Oblique-Slip Mobile Zones. United Kingdom: John Wiley & Sons, Ltd; p. 191–215.

Lowe DR. 1982. Sediment gravity flows; II, Depositional models with special reference to the deposits of high-density turbidity currents. Journal of Sedimentary Research. 52(1):279–297. https://doi.org/10.1306/212F7F31-2B24-11D7-8648000102C1865D

Maison T, Potel S, Malié P, Mählmann RF, Chanier F, Mahieux G, Bailleul J. 2018. Low-grade evolution of clay minerals and organic matter in fault zones of the Hikurangi prism (New Zealand). Clay Minerals. 53(4):579–602. https://doi.org/10.1180/clm.2018.46

Malie P, Bailleul J, Chanier F, Toullec R, Mahieux G, Caron V, Field B, Mählmann RF, Potel S. 2017. Spatial distribution and tectonic framework of fossil tubular concretions as onshore analogues of cold seep plumbing systems, North Island of New Zealand. Bulletin de la Société géologique de France. 188(4):25. https://doi.org/10.1051/bsgf/2017192

Maltman A. 1984. On the term "soft-sediment deformation." Journal of Structural Geology. 6(5):589–592. https://doi.org/10.1016/0191-8141(84)90069-5

McArthur AD, Bailleul J, Mahieux G, Claussmann B, Wunderlich A, McCaffrey WD. 2021. Deformation-sedimentation feedback and the development of anomalously thick aggradational turbidite lobes: subsurface and outcrop examples from the Hikurangi Margin, New Zealand. Journal of Sedimentary Research. 91(4):362–389. https://doi.org/10.2110/jsr.2020.013

McArthur AD, Claussmann B, Bailleul J, McCaffrey W, Clare A. 2019. Variation in syn-subduction sedimentation patterns from inner to outer portions of deep-water fold and thrust belts: examples from the Hikurangi subduction margin of New Zealand. Geological Society, London, Special Publications. 490:285–310. https://doi.org/10.1144/SP490-2018-95

McArthur AD, Kneller BC, Souza PA, Kuchle J. 2016. Characterization of deep-marine channel-levee complex architecture with palynofacies: An outcrop example from the Rosario Formation, Baja California, Mexico. Marine and Petroleum Geology. 73:157–173. https://doi.org/10.1016/j.marpetgeo.2016.02.030

McCrory PA. 1995. Evolution of a trench-slope basin within the Cascadia subduction margin: the Neogene Humboldt Basin, California. Sedimentology. 42(2):223–247. https://doi.org/10.1111/j.1365-3091.1995.tb02100.x

McHargue T, Pyrcz MJ, Sullivan MD, Clark JD, Fildani A, Romans BW, Covault JA, Levy M, Posamentier HW, Drinkwater NJ. 2011. Architecture of turbidite channel systems on the continental slope: Patterns and predictions. Marine and Petroleum Geology. 28(3):728–743. https://doi.org/10.1016/j.marpetgeo.2010.07.008

Moncrieff ACM. 1989. Classification of poorly-sorted sedimentary rocks. Sedimentary Geology. 65(1):191–194. https://doi.org/10.1016/0037-0738(89)90015-8

Moore GF, Billman HG, Hehanussa PE, Karig DE. 1980. Sedimentology and Paleobathymetry of Neogene Trench-Slope Deposits, Nias Island, Indonesia. The Journal of Geology. 88(2):161–180.

Moore GF, Karig DE. 1976. Development of sedimentary basins on the lower trench slope. Geology. 4(11):693–697. https://doi.org/10.1130/0091-7613(1976)4<693:DOSBOT>2.0.CO;2

Moore PR. 1980. Late Cretaceous-Tertiary stratigraphy, structure, and tectonic history of the area between Whareama and Ngahape, eastern Wairarapa, New Zealand. New Zealand Journal of Geology and Geophysics. 23(2):167–177. https://doi.org/10.1080/00288306.1980.10424204

Moore PR. 1986. A revised Cretaceous-early Tertiary stratigraphic nomenclature for eastern North Island, New Zealand. Lower Hutt, New Zealand.

Morgans HEG. 2016. The Weber Formation at its type locality in Southern Hawke's Bay, and its distribution through the East Coast, North Island, New Zealand. [place unknown].

Morgans HEG, Hollis CJ. 2000. Cretaceous-Paleogene stratigraphy of southern Hawkes Bay: K/T boundary, late Paleocene and Oligocene event horizons. In: Conference field trip. Geological Society of New Zealand Miscellaneous Publication 107; p. 220–248.

van Morkhoven FPCM, Berggren WA, Edwards AS, Oertli HJ. 1986. Cenozoic cosmopolitan deep-water benthic Foraminifera. Pau, France: Elf Aquitaine.

Mortimer N. 1994. Origin of the Torlesse Terrane and Coeval Rocks, North Island, New Zealand. International Geology Review. 36(10):891–910. https://doi.org/10.1080/00206819409465494

Mortimer N. 2004. New Zealand's Geological Foundations. Gondwana Research. 7(1):261–272. https://doi.org/10.1016/S1342-937X(05)70324-5

Mortimer N, Rattenbury M, King P, Bland K, Barrell D, Bache F, Begg J, Campbell H, Cox S, Crampton J, et al. 2014. High-level stratigraphic scheme for New Zealand rocks. New Zealand Journal of Geology and Geophysics. 57(4):402–419. https://doi.org/10.1080/00288306.2014.946062

Moscardelli L, Wood L. 2015. Morphometry of mass-transport deposits as a predictive tool. GSA Bulletin. 128(1–2):47–80.

Mourgues R, Cobbold PR. 2006. Thrust wedges and fluid overpressures: Sandbox models involving pore fluids. Journal of Geophysical Research : Solid Earth. 111(B5):B05404. https://doi.org/10.1029/2004JB003441

Mulder T, Alexander J. 2001. The physical character of subaqueous sedimentary density flows and their deposits. Sedimentology. 48(2):269–299. https://doi.org/10.1046/j.1365-3091.2001.00360.x

Mulder T, Cochonat P. 1996. Classification of offshore mass movements. Journal of Sedimentary Research. 66(1):43–57. https://doi.org/10.1306/D42682AC-2B26-11D7-8648000102C1865D

Mutti E, Normark WR. 1991. An Integrated Approach to the Study of Turbidite Systems. In: Weimer P, Link MH, editors. Seismic Facies and Sedimentary Processes of Submarine Fans and Turbidite Systems. New York, America: Springer; p. 75–106. https://doi.org/10.1007/978-1-4684-8276-8_4

Naranjo-Vesga J, Ortiz-Karpf A, Wood L, Jobe Z, Paniagua-Arroyave JF, Shumaker L, Mateus-Tarazona D, Galindo P. 2020. Regional controls in the distribution and morphometry of deep-water gravitational deposits along a convergent tectonic margin. Southern Caribbean of Colombia. Marine and Petroleum Geology. 121:104639. https://doi.org/10.1016/j.marpetgeo.2020.104639

Nardin TR, Hein FJ, Gorsline DS, Edwards BD. 1979. A review of mass movement processes, sediment and acoustic characteristics, and contrasts in slope and base-of-slope systems versus canyon-fan-basin floor systems. SEPM Special Publication. 27:61–73.

Neef G. 1992. Turbidite deposition in five miocene, bathyal formations along an active plate margin, North Island, New Zealand: with notes on styles of deposition at the margins of east coast bathyal basins. Sedimentary Geology. 78(1):111–136. https://doi.org/10.1016/0037-0738(92)90116-9

Neef G. 1995. Cretaceous and Cenozoic geology east of the Tinui Fault Complex in northeastern Wairarapa, New Zealand. New Zealand Journal of Geology and Geophysics. 38(3):375–394. https://doi.org/10.1080/00288306.1995.9514664

Neef G. 1997. Stratigraphy, structural evolution, and tectonics of the northern part of the Tawhero Basin and adjacent areas, northern Wairarapa, North Island, New Zealand. New Zealand Journal of Geology and Geophysics. 40(3):335–358. https://doi.org/10.1080/00288306.1997.9514766

Nemec W. 1990. Aspects of Sediment Movement on Steep Delta Slopes. In: Collela A, Prior DB, editors. Coarse-Grained Deltas. Oxford, United Kingdom: John Wiley & Sons, Ltd; p. 29–73. https://doi.org/10.1002/9781444303858.ch3

Nemec W, Steel RJ. 1984. Alluvial and Coastal Conglomerates: Their Significant Features and Some Comments on Gravelly Mass-Flow Deposits. In: Koster EH, Steel RJ, editors. Sedimentology of Gravels and Conglomerates, Memoir 10. Canada: Canadian Society of Petroleum Geologists; p. 1–31.

Nicol A, Mazengarb C, Chanier F, Rait G, Uruski C, Wallace L. 2007. Tectonic evolution of the active Hikurangi subduction margin, New Zealand, since the Oligocene. Tectonics. 26(4):1–24. https://doi.org/10.1029/2006TC002090

Noda A. 2018. Forearc Basin Stratigraphy and Interactions With Accretionary Wedge Growth According to the Critical Taper Concept. Tectonics. 37(3):965–988. https://doi.org/10.1002/2017TC004744

Ogata K, Festa A, Pini GA, Alonso JL. 2019. Submarine Landslide Deposits in Orogenic Belts: Olistostromes and Sédimentary Mélanges. In: Ogata K, Festa A, Pini GA, editors. Submarine Landslides: Subaqueous Mass Transport Deposits from Outcrops to Seismic Profiles. America: American Geophysical Union (AGU); p. 1–26. https://doi.org/10.1002/9781119500513.ch1

Ogata K, Pogačnik Ž, Pini GA, Tunis G, Festa A, Camerlenghi A, Rebesco M. 2014. The carbonate mass transport deposits of the Paleogene Friuli Basin (Italy/Slovenia): Internal anatomy and inferred genetic processes. Marine Geology. 356:88–110. https://doi.org/10.1016/j.margeo.2014.06.014

Okada H. 1989. Anatomy of trench-slope basins: Examples from the Nankai Trough. Palaeogeography, Palaeoclimatology, Palaeoecology. 71(1):3–13. https://doi.org/10.1016/0031-0182(89)90026-6

Ortiz-Karpf A, Hodgson DM, Jackson CA-L, McCaffrey WD. 2017. Influence of Seabed Morphology and Substrate Composition On Mass-Transport Flow Processes and Pathways: Insights From the Magdalena Fan, Offshore Colombia. Journal of Sedimentary Research. 87(3):189–209. https://doi.org/10.2110/jsr.2017.10

Pearson PN, Olsson RK, Huber BT, Hemleben C, Berggren WA. 2006. Atlas of eocene planktonic foraminifera [Internet]. Pearson PN, Olsson RK, Huber BT, Hemleben C, Berggren WA, editors. Fredericksburg, USA: Cushman Foundation for Foraminiferal Research. https://orca.cardiff.ac.uk/15234/

Pettinga JR. 1982. Upper Cenozoic structural history, coastal Southern Hawke's Bay, New Zealand. New Zealand Journal of Geology and Geophysics. 25(2):149–191. https://doi.org/10.1080/00288306.1982.10421407

Pickering KT, Corregidor J. 2005. Mass transport complexes and tectonic control on confined basin-floor submarine fans, Middle Eocene, south Spanish Pyrenees. Geological Society, London, Special Publications. 244(1):51–74. https://doi.org/10.1144/GSL.SP.2005.244.01.04

Pini GA, Lucente CC, Cowan D, C.M. D, Dellisanti F, A. L, Negri A, Tateo F, M. D, M. M, Cantelli L. 2004. The role of olistostromes and argille scagliose in the structural evolution of the Northern Apennines. Pre-Congress Field Trip B13. Memorie Descrittive della Carta Geologica d'Italia. 63:B13.1-B13.40.

Posamentier HW, Kolla V. 2003. Seismic geomorphology and stratigraphy of depositional elements in deep-water settings. Journal of Sedimentary Research. 73(3):367–388.

Posamentier HW, Martinsen OJ. 2011. The Character and Genesis of Submarine Mass-Transport Deposits: Insights from Outcrop and 3D Seismic Data. In: Shipp RC, Weimer P, Posamentier HW, editors. Mass-Transport Deposits in Deepwater Settings. Oklahoma, America: SEPM; p. 7–38.

Posamentier HW, Walker RG. 2006. Deep-Water Turbidites and Submarine Fans. In: Posamentier HW, Walker RG, editors. Facies Models Revisited. Oklahoma, America: SEPM Special Publication 84; p. 397–520. https://doi.org/10.2110/pec.06.84

Raine JI, Beu A, Boyes A, Campbell H, Cooper R, Crampton J, Crundwell M, Hollis C, Morgans H, Mortimer N. 2015. New Zealand Geological Timescale NZGT 2015/1. New Zealand Journal of Geology and Geophysics. 58(4):398–403. https://doi.org/10.1080/00288306.2015.1086391

Rait G, Chanier F, Waters DW. 1991. Landward- and seaward-directed thrusting accompanying the onset of subduction beneath New Zealand. Geology. 19(3):230–233. https://doi.org/10.1130/0091-7613(1991)019<0230:LASDTA>2.3.CO;2

Raymond LA. 1984. Classification of melanges. In: Melanges: Their Nature, Origin, and Significance. Vol. 198. America: Geological Society of America; p. 7–20.

Scott GH, Bishop S, Burt BJ. 1990. Guide to some Neogene Globorotalids (Foraminiferida) from New Zealand. Lower Hutt, New Zealand: New Zealand Geological Survey.

Sloss CR, Tillquist S, McGill S, Penny T, Ballington C, Nothdurft L, Trofimovs J, Lawrence MJ, Schrank CE. 2021. Sedimentology and stratigraphy of syn-subduction Miocene fine-grained turbidites deposited in first stages of trench-slope basin development: Whakataki Formation, North Island, New Zealand. Sedimentary Geology. 414:105819. https://doi.org/10.1016/j.sedgeo.2020.105819

Smith GW, Howell DG, Ingersoll RV. 1979. Late Cretaceous trench-slope basins of central California. Geology. 7(6):303–306. https://doi.org/10.1130/0091-7613(1979)7<303:LCTBOC>2.0.CO;2

Sobiesiak MS, Buso VV, Kneller B, Alsop GI, Milana JP. 2019. Block Generation, Deformation, and Interaction of Mass-Transport Deposits With the Seafloor. In: Submarine Landslides. Washington, America: American Geophysical Union (AGU); p. 91–104. https://doi.org/10.1002/9781119500513.ch6

Sobiesiak MS, Kneller B, Alsop GI, Milana JP. 2018. Styles of basal interaction beneath mass transport deposits. Marine and Petroleum Geology. 98:629–639. https://doi.org/10.1016/j.marpetgeo.2018.08.028

Spörli KB. 1978. Mesozoic tectonics, North Island, New Zealand. GSA Bulletin. 89(3):415–425. https://doi.org/10.1130/0016-7606(1978)89<415:MTNINZ>2.0.CO;2

Spörli KB. 1980. New Zealand and Oblique-Slip Margins: Tectonic Development up to and during the Cainozoic. In: Ballance PF, Reading HG, editors. Sedimentation in Oblique-Slip Mobile Zones. United Kingdom: John Wiley & Sons, Ltd; p. 147–170. https://doi.org/10.1002/9781444303735.ch9

Sprague AR, Garfield TR, Goulding FJ, Beaubouef RT. 2005. Integrated slope channel depositional models: the key to successful prediction of reservoir presence and quality in Offshore West Africa. In: Proceedings of the CIPM conference. Vol. 5. Veracruz, Mexico; p. 1–13.

Stevens SH, Moore GF. 1985. Deformational and sedimentary processes in trench slope basins of the western Sunda Arc, Indonesia. Marine Geology. 69(1):93–112. https://doi.org/10.1016/0025-3227(85)90135-5

Stow DAV. 1986. Deep clastic seas. In: Reading HG, editor. Sedimentary Environments and Facies. 2nd edition. Oxford, United Kingdom: Blackwell Scientific Publications; p. 399–444.

Stow DAV, Shanmugam G. 1980. Sequence of structures in fine-grained turbidites: Comparison of recent deep-sea and ancient flysch sediments. Sedimentary Geology. 25(1):23–42. https://doi.org/10.1016/0037-0738(80)90052-4

Strasser M, Moore GF, Kimura G, Kopf AJ, Underwood MB, Guo J, Screaton EJ. 2011. Slumping and mass transport deposition in the Nankai fore arc: Evidence from IODP drilling and 3-D reflection seismic data. Geochemistry, Geophysics, Geosystems. 12(5):1–24. https://doi.org/10.1029/2010GC003431

Suggate RP. 1961. Rock-stratigraphic names for the South Island schists and undifferentiated sediments of the New Zealand geosyncline. New Zealand Journal of Geology and Geophysics. 4(4):392–399. https://doi.org/10.1080/00288306.1961.10420127

Sylvester Z, Pirmez C, Cantelli A. 2011. A model of submarine channel-levee evolution based on channel trajectories: Implications for stratigraphic architecture. Marine and Petroleum Geology. 28(3):716–727. https://doi.org/10.1016/j.marpetgeo.2010.05.012

Taira A, Hill I, Firth J, Berner U, Brückmann W, Byrne T, Chabernaud T, Fisher A, Foucher J-P, Gamo T, et al. 1992. Sediment deformation and hydrogeology of the Nankai Trough accretionary prism: Synthesis of shipboard results of ODP Leg 131. Earth and Planetary Science Letters. 109(3):431–450. https://doi.org/10.1016/0012-821X(92)90104-4

Talling PJ. 2013. Hybrid submarine flows comprising turbidity current and cohesive debris flow: Deposits, theoretical and experimental analyses, and generalized models. Geosphere. 9(3):460–488. https://doi.org/10.1130/GES00793.1

Terry RD, Chilingar GV. 1955. Summary of Concerning some additional aids in studying sedimentary formations, by M. S. Shvetsov. Journal of Sedimentary Research. 25(3):229–234. https://doi.org/10.1306/74D70466-2B21-11D7-8648000102C1865D

Turnbull RJ. 1988. The geology of the lower Miocene Whakataki formation, eastern Wairarapa [MSc Thesis]. Wellington, New Zealand: Victoria University.

Underwood MB, Bachman SB. 1982. Sedimentary facies associations within subduction complexes. Geological Society, London, Special Publications. 10(1):537–550. https://doi.org/10.1144/GSL.SP.1982.010.01.35

Underwood MB, Moore GF. 1995. Trenches and trench-slope basins. In: Busby CJ, Ingersoll RV, editors. Tectonics of sedimentary basins. Oxford, United Kingdom: Blackwell Science; p. 179–219.

Underwood MB, Moore GF, Taira A, Klaus A, Wilson M, Fergusson C, Hirano S, Steurer J. 2003. Sedimentary and Tectonic Evolution of a Trench-Slope Basin in the Nankai Subduction Zone of Southwest Japan. Journal of Sedimentary Research. 73:589–602. https://doi.org/10.1306/092002730589

Underwood MB, Norville CR. 1986. Deposition of sand in a trench-slope basin by unconfined turbidity currents. Marine Geology. 71(3):383–392. https://doi.org/10.1016/0025-3227(86)90080-0

Van den Heuvel HB. 1960. The geology of the flat point area, eastern Wairarapa. New Zealand Journal of Geology and Geophysics. 3(2):309–320. https://doi.org/10.1080/00288306.1960.10423603

Vinnels JS, Butler RWH, McCaffrey WD, Paton DA. 2010. Depositional processes across the Sinú Accretionary Prism, offshore Colombia. Marine and Petroleum Geology. 27(4):794–809. https://doi.org/10.1016/j.marpetgeo.2009.12.008

Waldron JWF, Gagnon J-F. 2011. Recognizing soft-sediment structures in deformed rocks of orogens. Journal of Structural Geology. 33(3):271–279. https://doi.org/10.1016/j.jsg.2010.06.015

Watson SJ, Mountjoy JJ, Crutchley GJ. 2020. Tectonic and geomorphic controls on the distribution of submarine landslides across active and passive margins, eastern New Zealand. Geological Society, London, Special Publications. 500:477–494. https://doi.org/10.1144/SP500-2019-165

White RS, Louden KE. 1982. The Makran Continental Margin: Structure of a Thickly Sedimented Convergent Plate Boundary: Convergent Margins: Field Investigations of Margin Structure and Stratigraphy. 110:499–518.

Woodcock NH. 1979. The use of slump structures as palaeoslope orientation estimators. Sedimentology. 26(1):83–99. https://doi.org/10.1111/j.1365-3091.1979.tb00339.x

9. TABLES

Deposit	Dominant lithology	Lithofacies code	Thickness (cm)	Lithofacies description	Classification and process interpretation	
Turbidite	Sandstone to Mudstone	**LDTC** Tabular, very thin-to medium-bedded sandstone with mudstone cap	1 to 25 (sand) 2 to 100 (mud)	Fine- to medium-grained. Parallel laminations, passing into climbing ripples with sometimes dewatering or soft sedimentation deformation structures installed above. Sometimes only developing the parallel laminations or sometimes directly developing the climbing ripples. Laminations can be highlighted by organic-rich, carbonaceous debris. Sometimes displaying sole marks such as flute casts. Rare bioturbation in the mud cap.	Tb-e Tb-Te Tc-Te Tbc-Te	Low-density turbidity currents and hemipelagites
		HDTC Lenticular, medium to very thick-bedded sandstone with mudstone cap	50 to 1,500 (sand) 80 to 2,000 (mud)	Fine- to coarse-grained. Broadly lenticular, slightly to highly erosive, coarse- to very-coarse-grained base, commonly massive and structureless, with sand- to granule-grade clasts (lithoclasts and (elongated) rip-up mudstone clasts), overlain by well-developed parallel and or cross-laminations in the same material, overall normally grading. Followed by commonly very-thick, fine- to medium-grained intervals with well-developed parallel laminations, climbing ripples with frequent dewatering or soft sedimentation deformation structures (convolutes) installed above. Ending with thin regular, wispy and or convolute laminations in silty to very-fine grained material, overlain by normally graded, frequently including patchy silt pseudonodules, to ungraded mudstone cap. Rare bioturbation. Very calcareous, white to pale yellow sandstones. Very frequent amalgamation, commonly arising in the fine- to medium-grained and muddy intervals.	Ta-e	High to low-density turbidity currents and hemipelagites
Debrite	Conglomerate	**CF** Disorganized clast-supported	300 to 600 (2)	Clast-supported, siltstone to silty mudstone with ≤90% of granule- to boulder-grade extra- and intraformational clasts. Ungraded, disorganized. Common load structures.	/	Cohesionless debris flow
		DF Disorganized matrix-supported	200 to 300 (1) 150 to > 20,000 (2)	Matrix-supported, siltstone to silty mudstone with varying quantity of granule- to boulder-grade extra- and intraformational clasts. Ungraded, disorganized. Common recumbent folds, shear and load structures. Traction carpet possible.	/	Cohesive debris flow

Accepted Manuscript version. Published Journal Article version available online, published by Elsevier in Marine and Petroleum Geology Journal: https://doi.org/10.1016/j.marpetgeo.2023.106191

		MF Disorganized matrix-supported	150 to > 20,000 (2)	Matrix-supported, dominated by ≤95% of silty mudstone to mudstone, otherwise including granule- to boulder-grade extra- and intraformational clasts. Ungraded, disorganized. Common recumbent folds, shear and load structures. Traction carpet possible.	/	Cohesive mudflow
Displaced or contorted strata	Alternating sandstone and mudstone	**SL-a** Deformed mass of sediments	100 to > 10,000	Contorted, remobilized facies characterized by recumbent folds. When present, sandy to silty mudstone background facies.	/	Soft-sediment deformation: (1) gravity-driven = coherent mass of sediment that moves along a glide plane, resulting in significant internal deformation, *i.e.,* slump; or (2) tectonic-driven = folding
		SL-b Undeformed mass of sediments	1,000 to > 10,000	Coherent, remobilized facies displaying sharp truncations, slightly concave-up geometries with downlap.	/	Soft-sediment deformation: (1) gravity-driven, initiation of movement of a coherent mass of sediment along a glide plane, no to very little internal deformation, *i.e.,* slide; or (2) tectonic-driven

Table 1: Lithofacies encountered at the Pahaoa, Flat Point, Orui, Waimimi and Suicide Point-Mataikona coastal outcrops. See Figure 7 for representative photographs of each lithofacies. (1) Conglomerates observed at Pahaoa, Flat Point and Waimimi, (2) conglomerates observed at Orui and Suicide Point. 'Classification' column refers to Bouma (1962), Stow and Shanmugam (1980) and Lowe (1982).

Depositional system	Facies association code	Facies association sub-code	Facies assemblage description	Thickness (m)	Interpretation
Turbidite system	Fa1	Fa1w	HDTC interbedded with LDTC. HDTC frequently amalgamated, with thick mud caps, and truncating underlying LDTC. LDTC frequently displaying wedging geometries with low-angle downlap terminations within interval or onto HDTC mud caps. Occasionally interrupted by standalone DF from coevally developping mass-wasting system (Fa3n). Common shear zones.	400 (Waimimi-2) 270 (Waimimi-1) 100 (Flat Point)	Channel-levee system
Mass-wasting system	Fa3	Fa3n	Intertwined, coalescing DF and MF, reworking extraformational lithoclasts derived from the pre-subduction margin series and intraformational lithoclasts from the contemporaneously developing syn-subduction strata. Rare CF. Common ductile and brittle-ductile deformation fabrics. *First style:* mostly (>80%) Paleocene and Eocene extraformational clasts from pelagic units. Coeval to Fa1w. *Second style:* Cretaceous to Eocene extraformational clasts from intermediary units, overall being incorporated progressively in a reverse stratigraphic order. Overlying Fa1w.	*First style* up to 3 (Waimimi, Flat Point) 40 (Pahaoa) *Second style* ~500 (Suicide Point) 400 to 900 (Orui)	Dismantlement of advancing thrust sheet *First style:* from thrust sheet developed in the pelagic units of the pre-subduction margin series *Second style:* from thrust sheet developed in the intermediary units of the pre-subduction margin series
		Fa3s	Intertwined SL-a and or SL-b. Varying folding styles including widely open upright folds, narrow recumbent folds as well as curvilinear and rootless folds. Preferential general direction of fold axis and hinge. Underlying Fa3n.	300 (Orui)	Large-scale soft-sediment deformation of the previously deposited and poorly lithified sediments linked to advancing thrust nappe

Table 2 : Facies associations encountered at the Pahaoa, Flat Point, Orui, Waimimi and Suicide Point-Mataikona coastal outcrops. See Figure 8, Figure 9, Figure 11, Figure 12 and Figure 13 for representative photographs of each facies assemblage. The nomenclature leverages and complements the one that was defined by Bailleul et al. (2007) and Bailleul et al. (2013), and where **Fa1** are associated to turbidite systems and **Fa3** to mass-wasting deposits.

10. SUPPLEMENTARY MATERIAL

Supplementary data, namely Appendix 1 to 5, to this article can be found online at https://doi.org/10.1016/j.marpetgeo.2023.106191.

Appendix 1: Enlarged view of the southern part (w-1) of the Waimimi outcrop model, annotated with detailed paleocurrent analysis for each of the channel and levee-overbank settings (see Figure 5 for exact location of w-1 section).

Appendix 2: Enlarged view of the northern part (w-2) of the Waimimi outcrop model, annotated with detailed paleocurrent analysis for each of the channel and levee-overbank settings (see Figure 5 for exact location of w-2 section).

Appendix 3: Sample list for the Castlepoint trench-slope basin outcrops. The Fossil Record numbers including "T27" and "U26" respectively relate to the T27 and U26 New Zealand Map Grid 1:50,000 series and are captured in the Fossil Record Electronic Database FRED (https://fred.org.nz/) (Clowes et al. 2021). The Fossil Record numbers including "CZ" come from Chanier (1991) and are unpublished in FRED. See the respective Table 1 for the description of the lithofacies codes. The age of the sedimentary units and the paleobathymetries were defined using micro and macropaleontological analyses conducted by GNS Science New Zealand. (Jenkins 1971; Hornibrook et al. 1989; Scott et al. 1990; Cooper 2004; Pearson et al. 2006) and GNS file were used for the foraminiferal age determinations, and (Hayward and New Zealand Geological Survey Paleontology Group 1986; van Morkhoven et al. 1986; Crundwell et al. 1994; Hayward et al. 2012) and GNS file for the paleodepth interpretations. The general margin of error for the paleodepth interpretations is 30 meters error for 0 to 200 meters, 50 meters error for 200 to 600 meters, 100 meters error for 600 to 1000 meters and 200 meters error above 1000 meters.

Appendix 4: Thin section photographs from sample 20_12_09 corresponding to a limestone clast taken in the Orui mass-transport deposits, and more particularly in the mass-transport deposits d2 (see Figure 11, d2; Appendix 3). The identification of pithonellids (p) allows to discard an origin from the Paleocene limestones and instead suggests reworking of the Upper Cretaceous pithonellid-bearing limestones previously identified along the coastal ranges by (Chanier et al. 1990).

Appendix 5: Morphometric parameter calculations for the Pahaoa, Flat Point, Orui and Suicide Point mass-transport deposits using the equations from (Moscardelli and Wood 2015), where V = volume, A = area, L = length, T = thickness. (d) indicates that these equations were specifically created for *detached* mass-transport deposits.